34324

National Library of Canada
Bibliothèque nationale du Canada

CANADIAN THESES ON MICROFICHE

THÈSES CANADIENNES SUR MICROFICHE

NAME OF AUTHOR/*NOM DE L'AUTEUR* L. W. DIEHL

TITLE OF THESIS/*TITRE DE LA THÈSE* DYNAMICS OF BAROCLINIC WAVES AND BLOCKING RIDGE DEVELOPMENT

UNIVERSITY/*UNIVERSITÉ* UNIVERSITY OF ALBERTA

DEGREE FOR WHICH THESIS WAS PRESENTED/ *GRADE POUR LEQUEL CETTE THÈSE FUT PRÉSENTÉE* MSc.

THIS DEGREE CONFERRED/*ANNÉE D'OBTENTION DE CE GRADE* 1977

NAME OF SUPERVISOR/*NOM DU DIRECTEUR DE THÈSE* DR K.D. HAGE

Permission is hereby granted to the NATIONAL LIBRARY OF CANADA to microfilm this thesis and to lend or sell copies of the film.

The author reserves other publication rights, and neither the thesis nor extensive extracts from it may be printed or otherwise reproduced without the author's written permission.

L'autorisation est, par la présente, accordée à la BIBLIOTHÈQUE NATIONALE DU CANADA de microfilmer cette thèse et de prêter ou de vendre des exemplaires du film.

L'auteur se réserve les autres droits de publication; ni la thèse ni de longs extraits de celle-ci ne doivent être imprimés ou autrement reproduits sans l'autorisation écrite de l'auteur.

DATED/*DATÉ* October 21 1977 SIGNED/*SIGNÉ* L W Diehl

PERMANENT ADDRESS/*RÉSIDENCE FIXÉ* 9625 76 AVE EDMONTON ALBERTA

NL-91 (3-74)

National Library of Canada

Cataloguing Branch
Canadian Theses Division

Ottawa, Canada
K1A 0N4

Bibliothèque nationale du Canada

Direction du catalogage
Division des thèses canadiennes

NOTICE

The quality of this microfiche is heavily dependent upon the quality of the original thesis submitted for microfilming. Every effort has been made to ensure the highest quality of reproduction possible.

If pages are missing, contact the university which granted the degree.

Some pages may have indistinct print especially if the original pages were typed with a poor typewriter ribbon or if the university sent us a poor photocopy.

Previously copyrighted materials (journal articles, published tests, etc.) are not filmed.

Reproduction in full or in part of this film is governed by the Canadian Copyright Act, R.S.C. 1970, c. C-30. Please read the authorization forms which accompany this thesis.

THIS DISSERTATION
HAS BEEN MICROFILMED
EXACTLY AS RECEIVED

AVIS

La qualité de cette microfiche dépend grandement de la qualité de la thèse soumise au microfilmage. Nous avons tout fait pour assurer une qualité supérieure de reproduction.

S'il manque des pages, veuillez communiquer avec l'université qui a conféré le grade.

La qualité d'impression de certaines pages peut laisser à désirer, surtout si les pages originales ont été dactylographiées à l'aide d'un ruban usé ou si l'université nous a fait parvenir une photocopie de mauvaise qualité.

Les documents qui font déjà l'objet d'un droit d'auteur (articles de revue, examens publiés, etc.) ne sont pas microfilmés.

La reproduction, même partielle, de ce microfilm est soumise à la Loi canadienne sur le droit d'auteur, SRC 1970, c. C-30. Veuillez prendre connaissance des formules d'autorisation qui accompagnent cette thèse.

LA THÈSE A ÉTÉ
MICROFILMÉE TELLE QUE
NOUS L'AVONS REÇUE

THE UNIVERSITY OF ALBERTA

DYNAMICS OF BAROCLINIC WAVES AND BLOCKING RIDGE DEVELOPMENT

by

© LAWRENCE WAYNE DIEHL

A THESIS

SUBMITTED TO THE FACULTY OF GRADUATE STUDIES AND RESEARCH
IN PARTIAL FULFILMENT OF THE REQUIREMENTS FOR THE DEGREE
OF MASTER OF SCIENCE

IN

METEOROLOGY

DEPARTMENT OF GEOGRAPHY

EDMONTON, ALBERTA

FALL, 1977

THE UNIVERSITY OF ALBERTA

FACULTY OF GRADUATE STUDIES AND RESEARCH

The undersigned certify that they have read, and recommend to the Faculty of Graduate Studies and Research, for acceptance, a thesis entitled "Dynamics of Baroclinic Waves and Blocking Ridge Development", submitted by Lawrence Wayne Diehl in partial fulfilment of the requirements for the degree of Master of Science in Meteorology.

........Keith D. Hage........
Supervisor

........E R Reinelt........

....

Date ..OCTOBER 17...... 1977

Dedicated to

my loving wife and children

ABSTRACT

In this study a linear two-level baroclinic model is formulated in which the zonal steady-state current is perturbed by surface friction and surface sensible heat exchange. The perturbation quantities are assumed to be either independent of latitude or varying sinusoidally with latitude.

Investigation of the phase velocity response of the model indicates that sensible heat exchange decreases the amount of instability of short and intermediate waves, but increases the longwave instability. The combined influence of friction and diabatic heating is to create unstable long waves which travel eastwards at reduced speeds and which may be stationary or retrogressive in nature depending on the speed of the mean zonal current.

Phase and amplitude characteristics of the existing perturbation waves suggest that the thermal wave necessarily lags the geopotential wave during amplification while the static stability wave prefers a lead position. In addition, maximum downward vertical velocity and maximum surface sensible heat transfer to the atmosphere occur between the ridge and downstream trough position.

It has been suggested that blocking ridges may be a form of longwave baroclinic instability and that sensible heat transfer plays an important role in their formation. Comparison of numerical predictions of unstable longwave

amplification with observed North Pacific blocking space and time scales indicates that without the presence of sensible heating in the model the development of blocking waveforms is not feasible. With sensible heat exchange stationary unstable waveforms are obtained which have growth times and wavelengths that are similar to observed North Pacific blocks.

ACKNOWLEDGEMENTS

I wish to thank Dr K. D. Hage for finding time in a busy schedule to supervise this study, and for having given valuable suggestions during its preparation.

I wish to express my appreciation to Dr. E. R. Reinelt for his assistance in the preparation of this thesis and for serving on my examining committee.

I also wish to thank Dr. E. Nyland for serving on my examining committee.

I am deeply grateful to Ms. Laura Smith for assisting in the preparation of the tables and captions in the thesis.

This study was conducted at the University of Alberta while on Educational leave from the Atmospheric Environment Service, Department of Fisheries and the Environment, Canada.

TABLE OF CONTENTS

Page

DEDICATION iv
ABSTRACT v
ACKNOWLEDGEMENTS vii
TABLE OF CONTENTS viii
LIST OF TABLES x
LIST OF FIGURES xi

CHAPTER

1 INTRODUCTION 1
  1.1 Theories on Blocking Ridge Formation 1
  1.2 Two-level Baroclinic Models 8
  1.3 Intentions of This Study .... 1[illegible]
2 DEVELOPMENT OF THE MODEL 13
  2.1 Consistency in Energy and Vorticity 13
  2.2 Sensible Heating and Static Stability 18
  2.3 Frictional Terms 23
  2.4 The Model Equations 24
3 NUMERICAL PROCEDURE 27
  3.1 Boundary Conditions and Coefficient Values 27
  3.2 Perturbation Equations 32

3.3 Stability Analysis 39

3.4 Wave Dynamics 44

4 NUMERICAL RESULTS AND DISCUSSION 49

4.1 Preliminary Comments 49

4.2 Influence of Sensible Heating and Friction on Dynamic Stability 50

4.3 Variation of the Steady-state Flow Parameters 59

4.4 Perturbation Field as a Function of Latitude 63

4.5 Amplitude and Phase Relationships 69

4.6 Blocking Ridge Development Over the North Pacific 80

5 SUMMARY AND CONCLUSIONS 99

REFERENCES 104

LIST OF TABLES

Table	Description	Page
1	Stability classification	43
2	Unstable waveband of model 1	52
3	Unstable waveband of model 2	53
4	Unstable waveband from Haltiner (1967)	55
5	Unstable waveband of model 3	57
6	Unstable waveband of model 4	58
7	Unstable waveband of the full model with a 90° meridional wavelength	67
8	Stationary unstable waves of model 2	89
9	Stationary unstable waves of model 3	91
10	Stationary unstable waves of model 4	92
11	Stationary unstable waveband of model 4 for increased vertical wind shear	93
12	Unstable waveband of the full model for varying meridional wavelengths	96
13	Stationary unstable waveband of the full model for increased vertical wind shear	97

LIST OF FIGURES

Figure Page

1.1 Dispersion of an initial solitary wave 3

1.2 Two-dimensional current of the hydraulic jump analogue model 6

2.1 Lorentz (1960) two-level model 22

3.1 Deviation of the sea-level pressure field from the bottom of the model 37

4.1 Phase velocity as a function of wavelength for models 1 and 2 51

4.2 Phase velocity as a function of wavelength for models 3 and 4 56

4.3 Effect on dynamic stability of changes in the surface sensible heating rate 60

4.4 Effect on dynamic stability of changes in the vertical wind shear and static stability 62

4.5 Effect of latitude variations on dynamic stabilty 64

4.6 Phase velocity response of the full model with a meridional wavelength of 90° ... 66

4.7 Effect on dynamic stability of varying the meridional wavelength 68

4.8 Amplitude and phase relationships of an intermediate wave: Case 1 71

4.9 Amplitude and phase relationships of an intermediate wave: Case 2 73

4.10 Amplitude and phase relationships of a long wave: Case 1 76

4.11 Amplitude and phase relationships of a long wave: Case 2 77

4.12 Seasonal and spatial variability of North Pacific blocking 82

4.13 Phase speed curves of Haltiner (1967) 83

4.14 January zonal winds over the Northern Hemisphere 85

4.15 Winter zonal wind profile at 45N............ 86

CHAPTER 1

INTRODUCTION

1.1 Theories on Blocking-Ridge Formation

Blocking-ridge activity is one of the most visible forms of longwave growth in the atmosphere and has long been recognized as being a major influence on regional climate. Such enduring ridge formations, which are found to be more frequent and pronounced during the winter, can displace passing synoptic disturbances considerable distances to the north or south of normal storm tracks. This then invariably leads to anomalies in such parameters as surface temperature and precipitation when compared to the non-blocking regime. Although the climatic effects and behavior of blocking ridges have been well documented, the dynamic causes surrounding their initial formation and development are still not fully understood.

In an early consideration of blocking phenomena, Yeh (1949) suggested that the transfer of energy by dispersive waves in the atmosphere might explain the occurrence of sustained ridging. These waves are created by a process of rapid adjustment between the pressure and velocity fields and energy propagation occurs at a group velocity which can be very different from the speed of the prevailing westerly current. By examining the characteristics of a solitary wave within an incompressible uniform atmosphere, it was shown that once a pressure rise or fall was created near the pole it would remain there without being dispersed. At latitudes other than the pole the solitary pressure wave was found to retrogress while slowly spreading out and dispersing, a characteristic often exhibited by atmospheric blocks. From these results it was concluded that blocking activity was likely a high-latitude feature of atmospheric flow which has greater intensity, a longer lifetime and moves with slower velocities as latitude increases.

Although this concept can describe a few of the prominent properties of the blocking process it represents others inaccurately. For instance it overpredicts both the extent of the motion and the rate of dispersion of blocking ridges at lower and middle latitudes. Figure 1.1 illustrates the behavior of a solitary dispersive wave at 40N and 70N. The curve representing the theoretical results for 40N shows that after a relatively brief period of 32 hours the wave amplitude has dropped to 1/3 of its initial value and has moved upstream more than 6000 km. At 70N after two days the same solitary wave had retrogressed at an average speed of 880 km/day and its amplitude had diminished by approximately 1/6 of its original value. The characteristics of the wave at 40N are not representative of actual blocking behavior, while the wave speed and dispersion rate at 70N are more indicative of the last

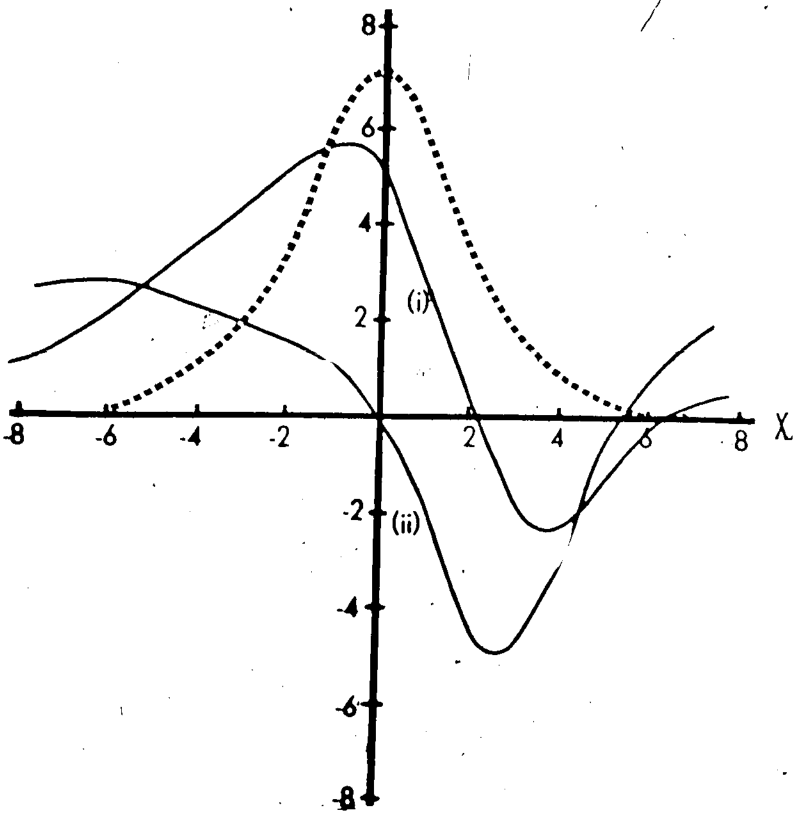

Fig. 1.1. Dispersion of an initial solitary wave. The dashed curve is the initial waveform at time t = 0; curve (i) is the wave profile at latitude 40N after approximately 32 hours and curve (ii) is the wave profile as seen at 70N after approximately 2 days. The abscissa is in units of 2200 km, while the ordinate is in arbitrary non-dimensional units of amplitude. The rate of dispersion of the wave amplitude at both latitudes increased significantly as time progressed. The speed of the retrogression at 70N remained constant, however, accelerated retrogression was observed at 40N as time went on. Curves are taken from Yeh (1949).

stages of blocking when the ridge is deteriorating. In general the theory does not describe satisfactorily the development or persistence aspects of the phenomenon nor does it explain why atmospheric blocks tend to show a longitudinal and seasonal preference in their formation.

Other investigators such as Berggren, Bolin and Rossby (1949) have hypothesized that blocking in the form of a wave-like perturbation could be analogous to that of a hydraulic jump in open channel flow. Continuing this approach, Rex (1950a) employed a hydraulic analogue model as devised by Rossby (1950) and a momentum transfer argument to arrive at a critical velocity given by

$$u_c = \beta \frac{a^2}{3} \qquad (1.1.1)$$

where β is the linear Beta-plane approximation to the north-south variation in the Coriolis parameter f (i.e. $f(y)=f_0+\beta y$), and a is the half-width of the current flow. Whenever the actual zonal current speed exceeds u two permissible modes of flow exist with one being at a higher energy level and velocity than the other; a necessary condition for an analogy to a hydraulic jump. From (1.1.1) it is evident that decreasing the stream width and increasing its flow speed meant lowering the critical threshold of the flow such that an external impulse to the stream might cause the jump to a higher energy state. Therefore a region aloft with a narrow strong jet and anomalously low thickness values (shallow stream depth) would lend itself more easily to the formation of a blocking ridge. The propagation of the atmospheric 'jump' once it has formed was determined to be

$$c = N - n(n+1) \tag{1.1.2}$$

where $N=u/u_c$ is the critical velocity ratio, u is the immediate upstream current velocity, and $n=a_1/a$ is the expansion ratio of the upstream and downstream current half-widths as indicated in Figure 1.2.

After applying the theory to a number of test cases, Rex (1950a) concluded that no major contradictions were apparent and that the concept gave credible results in predicting when blocking might occur. However, one argument made against the hydraulic jump theory is that it lacks a feasible energy source required to excite and then maintain the developed wave state associated with occurrences of blocking in the atmosphere. There is also some question as to how applicable the idea of a finite current width is to the real atmosphere. In narrow 'well-defined' stream widths when the term a is small, calculations of u are apt to be unrealistically small and the resulting inordinately large values of N and n do not lead to the correct interpretation of blocking behavior. In situations when the flow boundaries are not so well-defined there is often some arbitrariness in the selection of the half-width and therefore some uncertainty about the value of the predictions.

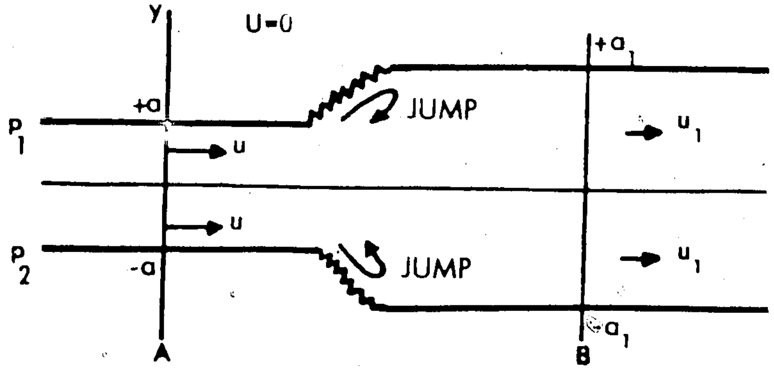

Fig. 1.2. The simple two-dimensional steady current envisioned in the hydraulic jump analogue model used by Rex (1950a). Zonal current speed u is assumed constant over the cross-section A, as is u_1 over cross-section B. The "jump" can occur according to the theory if $N = u/u_c > 1$, where the critical velocity is defined as $u_c = \beta a^2/3$. Current flow is assumed to vanish (U = 0) in the environment surrounding the channel.

In an investigation of the zonal index cycle, Namias (1950) alluded to the possiblity that blocking action was a manifestation of baroclinic instability in the atmosphere. Later, after studying the interactions of an ocean-atmosphere environment, Namias (1959) proposed that the thermal energy anomalies contained in the upper ocean may provide the necessary energy source for occurrences of mid-ocean blocking. Other studies on sea-atmosphere heat transfers, however, have indicated that fluctuations in the ocean's surface temperature do not normally play an active role in governing thermal energy exchanges on a time scale such as is associated with the development of blocking ridges (Kraus and Morrison, 1966; Clark, 1967). It would seem that sensible heat transfer in response to surface air temperature fluctuations could form a more viable energy source having a suitable time scale of several days to several weeks.

Theoretical results which have been interpreted as supporting the baroclinic instability concept of blocking-ridge formation came from work done by Haltiner (1967). Using a linearized two-level baroclinic model he has indicated that with the input of sensible heating from the surface a region of possible stationary or retrograde unstable wave growth is created for longer wavelengths in the range of 7000-9000 km. The instability of long waves in general was found to increase gradually as the amount of sensible heating was increased while waves on a near-synoptic scale became slightly more stable. These results were obtained for representative 50 kilopascal level winter values at mid-latitudes.

Encouraged by this theoretical evidence, White and Clark (1975) examined monthly mean atmospheric data taken over the North Pacific covering a period of 1950-1970. Their study found that blocking action was most often observed over the North Pacific ocean at a longitude of 160W to 170W with a dominant space scale of 6000 to 7000 km. In addition they were to discover that the distribution of anomalous surface sensible heat flux was strongly correlated with the anomalous 70 kPa heights associated with the development of blocking ridges. Below normal heating values were found to occur under the position of the ridging and above normal sensible heat exchange was associated with the adjacent trough regions on either side of the block. It was the conclusion of these investigators that sensible heat exchange between the ocean and the atmosphere was likely very important in the formation of blocking ridges and that the application of baroclinic instability theory to this type of phenomenon seemed plausible.

1.2 Two-level Baroclinic Models

Many of the baroclinic models which have been utilized in numerical prediction are of a simple two-level design. The procedure usually consists of applying a vorticity equation at two isobaric levels in the modelled atmosphere, (e.g. 25 kPa and 75 kPa) and a thermodynamic equation at an intermediate level, (50 kPa). The sum and the difference of the vorticity equations over the upper and lower information levels constitute averaged and thermal equations, respectively. The system of equations is then closed by an equation of state. Analysis of the dynamics of the model is possible by employing perturbation wave solutions with which the equations are reduced to that of the linear type and a frequency equation is obtained.

Early studies using this approach assumed that the motions in the atmosphere were both adiabatic and frictionless. Using a quasi-geostrophic linearized two-level model, Holopainen (1961) was able to incorporate the effects of surface friction into his perturbation equations. For adiabatic frictionless flow, using representative atmospheric values, it had been established that the perturbation field contained a unstable component over a small range of relatively short wavelengths. The effect of introducing surface friction was to broaden this range slightly while reducing the component amplitude of the previously-existing unstable wavelengths. Haltiner and Calverly (1965) using a similar formulation investigated the influence of surface-based friction on the interactions between the averaged wave and the thermal wave. Their study gave evidence that the phase characteristics of the two waves were markedly affected by friction. Results showed that decreases in the limiting phase difference were predicted when the value of the surface drag coefficient was increased.

Applying a different formulation of the hydrodynamic equations, Lorenz (1960) designed a two-level non-geostrophic model which allowed for full variability in the Coriolis parameter and the static stability. Gates (1961) has investigated the linearized form of this model under conditions of frictionless adiabatic flow. His results suggested that the unstable perturbation component was significantly larger using a variable static stability than for cases in the usual quasi-geostrophic formulation when this stability parameter was held constant. The perturbation equations as derived in this study formed the basis for the previously-mentioned investigation into sensible heat influences on baroclinic instability by Haltiner (1967).

The dynamics of baroclinic waves have not been investigated by analytical methods alone. Kikuchi (1969, 1971) used spherical harmonics for the time integration of the vorticity and thermodynamic equations in a quasi-geostrophic two-level model. These numerical investigations were aimed directly at reproducing the occurrence of blocking action and at gaining a better understanding of the effects of diabatic heating and mountain ranges on the behavior of such longwave growth. Included in the diabatic heating were the release of latent heat and radiational flux divergence as well as sensible heat exchange. Numerical computations showed that quasi-stationary longwave amplification similar to blocking processes occurred in the model whether orography was included or not. The main effect of the inclusion of mountains in the model was to lengthen slightly the duration of the computed ridging and to create preferred longitudinal regions where blocking occurred more frequently.

1.3 Intentions of This Study

In this study a two-level baroclinic model which incorporates a variable static stability will be developed. Terms which will describe the input of surface sensible heating as well as lateral and vertical turbulent heat flux in the atmosphere are included. The effects of introducing surface friction at the lower boundary of the atmosphere and those friction terms arising from turbulent diffusion by small eddies within the current flow will also be examined.

The governing equations will be linearized by neglecting squares and products of the perturbation variables. The dynamic features of the linear model will then be analyzed. The emphasis of this analysis will be on the stability of the baroclinic waves in response to varying values of sensible heating, friction and other variables as well as the interactions between perturbation waves.

Of particular interest, in view of the findings of White and Clark (1975), will be the behavior of the so-called long wavelengths in the possibility of explaining some aspects of blocking-ridge development. It cannot be expected, however, that any perturbation method will be able to portray accurately all of the characteristics of the longwave amplification we observe in the real atmosphere such as those found in the blocking process. One feature that may be difficult to explain by perturbation analysis is the persistence of blocks. After having gone through a period of unstable growth, the ridge can be seen to remain in a non-amplifying developed state for an extended length of time, implying that some form of stable mode is accquired. It seems likely that this is beyond the prediction capability of a linearized model and, therefore, what will be of prime concern in this study is the period of time when instability is realized and wave amplitude increases to a developed state.

CHAPTER 2

DEVELOPMENT OF THE MODEL

2.1 Consistency in Energy and Vorticity

In designing a simple baroclinic model some manner of modification is required to reduce the system of hydrodynamic equations to a less complicated form. In order to yield what would still be considered compatible results it is desirable that the reduced relations are consistent with any conservation principles expressed by the exact equations. The governing equations which describe atmospheric motions exhibit several such principles regarding the production of relative vorticity and energy on a global basis. They are:

(a) the mean generation of relative vorticity over a global pressure surface is zero;

(b) total energy under reversible adiabatic processes is conserved; and

(c) the sum of the kinetic energy and the available potential energy is conserved.

One method of simplifying a given equation is to compare the magnitudes of the various terms within it and then neglect those which are of smaller order. The orders of magnitude of individual terms are based on time and space scale considerations of the phenomenon to which the equation is being applied. This approach is therefore called scale analysis and was introduced by Charney (1948). Application of the scale analysis technique while checking to maintain the integral vorticity and energy invariants allows the governing equations to be reduced in a consistent manner.

A reduction in the complexity of the equations can also be made by using some form of general approximation pertaining to the atmospheric velocity field. The type of approximation used in many models is the quasi-geostrophic assumption in which the horizontal velocity field and vertical component of relative vorticity are evaluated by the non-divergent geostrophic wind. Charney (1947) has shown that assuming the horizontal velocity to be geostrophic has the effect of filtering out high-speed inertia-gravitational waves which occur in the equations of motion and thereby a significant simplification is achieved. The conventional quasi-geostrophic two-level baroclinic model (Charney and Phillips, 1953), however, has inherent energetic inconsistencies which result in prediction errors. For example, there is a tendency for the model to over-predict the amount of kinetic energy in the atmosphere. Such inconsistencies and their effect on the model's performance are discussed by Gates (1961).

A simplified set of dynamic equations which possesses certain consistent integral properties with respect to energy and vorticity has been formulated by Lorenz (1960). For a filtering approximation the quasi-geostrophic assumption was replaced by a relation known as the balance equation. This approximation is derived from the following form of the divergence equation

$$\nabla^2\phi - f\zeta + (\hat{k}\times\vec{V})\cdot\vec{\nabla}f - 2J(u,v) = 0 \qquad (2.1.1)$$

where is the geopotential, $\vec{V}$ is the horizontal wind for which u is the west-east x-component and v the south-north y-component, $\vec{\nabla} = \hat{i}\,\partial/\partial x + \hat{j}\,\partial/\partial y$, $\zeta = \vec{\nabla}\times\vec{V}$ is the vertical component of relative vorticity, $\hat{i}$, $\hat{j}$ and $\hat{k}$ are the unit vectors and J represents a Jacobian in the normal differential form. If a stream function ψ and a velocity potential χ are defined such that

$$\vec{V} = \vec{V}_\psi + \vec{V}_\chi \qquad (2.1.2)$$

$$\vec{V}_\chi = \vec{\nabla}\chi \qquad (2.1.3)$$

$$\vec{V}_\psi = \hat{k}\times\vec{\nabla}\psi \qquad (2.1.3)$$

in which $\vec{V}_\psi$ and $\vec{V}_\chi$ are the rotational and divergent portions of the horizontal wind, then (2.1.1) takes the form

$$\nabla^2\phi - \vec{\nabla}\cdot(f\vec{\nabla}\psi) + 2\left(\frac{\partial^2\psi}{\partial x\partial y}\right)^2 - 2\frac{\partial^2\psi}{\partial x^2}\frac{\partial^2\psi}{\partial y^2} = 0 \qquad (2.1.5)$$

Thus the balance equation as given by by (2.1.5) implies that a continual equilibrium exists between the rotational portion of the wind and the geopotential field.

The prognostic equations used with (2.1.5) were the adiabatic thermodynamic equation and the vorticity equation neglecting friction. The former can be expressed as

$$\frac{d\theta}{dt} = \frac{\partial\theta}{\partial t} + \vec{V}\cdot\vec{\nabla}\theta + \omega\frac{\partial\theta}{\partial p} \qquad (2.1.6)$$

where $\omega = dp/dt$ represents vertical velocity, t is time and θ the potential temperature. Potential temperature at a given pressure p (kPa) and temperature T (°C) is given by the relation

$$\theta = \left(\frac{100}{p}\right)^{\kappa} T \qquad (2.1.7)$$

in which $\kappa = R/c_p$ is a dimensionless ratio of the specific gas constant of dry air R and the specific heat capacity of air at constant pressure c_p.

The version of the vorticity equation which was used can be written as

$$\frac{\partial\zeta}{\partial t} + \vec{V}\cdot\vec{\nabla}(\zeta+f) + \omega\frac{\partial\zeta}{\partial p} + (\zeta+f)\vec{\nabla}\cdot\vec{V}_{\chi} + \hat{k}\,\vec{\nabla}\omega \times \frac{\partial\vec{V}_{\psi}}{\partial p} = 0 \qquad (2.1.8)$$

By applying (2.1.2)-(2.1.4) relative vorticity can be related to the stream function by

$$\zeta = \vec{\nabla}\times\vec{V} = \vec{\nabla}\times\vec{V}_{\psi} = \nabla^2\psi \qquad (2.1.9)$$

In addition if δ represents horizontal divergence $\vec{\nabla}\cdot\vec{V}$, then

$$\delta = \nabla\cdot\vec{V}_{\chi} = \nabla^2\chi \qquad (2.1.10)$$

Therefore, under hydrostatic conditions defined by

$$\frac{\partial\phi}{\partial p} = -\frac{1}{\rho} \qquad (2.1.11)$$

where ρ is density, the continuity equation can be written in the following form

$$\delta + \frac{\partial\omega}{\partial p} = \nabla^2\chi + \frac{\partial\omega}{\partial p} = 0 \qquad (2.1.12)$$

Employing (2.1.2)-(2.1.4), (2.1.9) and (2.1.12) the prognostic equations (2.1.6) and (2.1.8) can be written as

$$\frac{\partial\theta}{\partial t} + J(\psi,\theta) + \vec{\nabla}(\theta\vec{\nabla}\chi) + \frac{\partial}{\partial p}(\omega\theta) = 0 \qquad (2.1.13)$$

$$\frac{\partial}{\partial t}\nabla^2\psi + J(\psi,\nabla^2\psi+f) + \vec{\nabla}\chi\cdot\vec{\nabla}(\nabla^2\psi+f) + \omega\frac{\partial}{\partial p}\nabla^2\psi + (\nabla^2\psi+f)\delta + \vec{\nabla}\omega\cdot\vec{\nabla}\frac{\partial\psi}{\partial p} = 0 \qquad (2.1.14)$$

Through a systematic analysis of the integral constraints, Lorenz (1960) has shown that together (2.1.5) and (2.1.14) have invariant energy and vorticity relations similar to the exact divergence and vorticity equations. Thus, with the addition of (2.1.13), they form an energetically-consistent system of equations.

This system of equations can be reduced further if the phenomenon to which the motions are being applied is of a synoptic or larger scale. After (2.1.14) is subjected to such a scale analysis (cf Haltiner, 1971) and smaller terms are omitted, a second approximation which maintains the integral vorticity constraint is

$$\frac{\partial}{\partial t}\nabla^2\psi + J(\psi,\nabla^2\psi+f) + \vec{\nabla}\chi\cdot\vec{\nabla}f - f\frac{\partial\omega}{\partial p} = 0 \qquad (2.1.15)$$

An equation originating from (2.1.5) which, when used with (2.1.15), satisfies the energy constraints is

$$\nabla^2\phi - \vec{\nabla}f\cdot\vec{\nabla}\psi - f\nabla^2\psi = 0 \qquad (2.1.16)$$

Equation (2.1.16) is sometimes called the 'linear' balance equation. The set of equations (2.1.13), (2.1.15) and (2.1.16) will form the basis for the model equations to be used in the present investigation.

It should be pointed out that for (b) and (c) to be true when hydrostatic conditions are assumed, the kinetic energy contained in the vertical component of the motion cannot be included in the overall total kinetic energy. However, it can be said that the amount neglected is an insignificant fraction of the total energy involved in synoptic and larger scale systems and, therefore, the omission is normally of small consequence.

2.2 Sensible Heating and Static Stability

In order to incorporate sensible heat exchange in the modelling the First Law of thermodynamics will be used in the form

$$c_p T \frac{d\ln\theta}{dt} = \dot{H} \qquad (2.2.1)$$

where $\dot{H}$ is the rate at which external heat is added per unit mass (i.e. $\dot{H}=dH/dt$). By applying (2.1.7) the First Law states that the total rate of change of potential temperature is

$$\frac{d\theta}{dt} = \left(\frac{p}{100}\right)^{-\kappa} \frac{\dot{H}}{c_p} \qquad (2.2.2)$$

This is simply the diabatic form of (2.1.13).

The rate and direction of sensible heat flow across the interface of any two adjacent environments is largely dictated by the local difference in the respective temperatures on either side. In the atmospheric situation, where the air is in motion over a comparatively fixed underlying surface, the speed and turbulent state of the overriding air flow are also of primary import in determining a heat exchange rate. An estimate of the turbulent exchange of sensible heat at the earth's surface can be made using

$$\dot{H}_s = C V_s (T_g - T_a) \qquad (2.2.3)$$

where T is the surface air temperature, T the underlying ground or sea temperature and V_s the surface wind speed. The term C is determined from atmospheric parameters (such as the surface drag coefficient) and is constant for a given value of V_s. Equation (2.2.3) is discussed in detail by Budyko (1956) and generally has been applied to calculations of turbulent heat transfers over water surfaces rather than over the continents. Haltiner (1967) has used this form of surface heat input in his model. As a further approximation, however, Haltiner (1967) assumed that the heating was distributed through the atmosphere according to a vertical profile of

$$\dot{H}(p) = \dot{H}\left(\frac{p}{p_s}\right)^r \qquad (2.2.4)$$

for which $\dot{H}(p)$ represents the rate of sensible heating occurring at pressure p, p_s is surface pressure and r is a constant taken to equal 2 for his investigation.

In the present study no assumptions will be made as to a predetermined vertical distribution for sensible heating. Rather, considerations of the turbulent nature of the atmosphere will be used to provide a mechanism for vertically transporting heat. The process of heat transport by turbulent eddies in the air is known as thermal turbulent diffusion. If $\dot{H}_j$ denotes the sensible heating rate at some level j in the modelled atmosphere then it can be separated intc two parts

$$\dot{H}_j = R_j + S_j \qquad (2.2.5)$$

where R and S are the vertical and horizontal turbulent thermal diffusion terms, respectively.

The vertical diffusion of sensible heat will be defined by

$$R_j = g\frac{\partial h_j}{\partial p} \qquad (2.2.6)$$

in which g is the gravitational acceleration. Here h_j represents the vertical heat flux given by

$$h_j = \rho^2 g c_p K_v \left[\left(\frac{\partial \theta_j}{\partial p}\right) - \Gamma \right] \qquad (2.2.7)$$

where K_v is the vertical kinematic eddy diffusivity coefficient and Γ (°C/kPa) acts as a measure of the countergradient. The concept of an atmospheric countergradient flux is used to explain observations of the occurrence of some upward heat flux even under slightly stable conditions. The lateral diffusion term is to be determined by

$$S_J = c_p K_H \nabla^2 T_J = c_p K_H \left(\frac{p_J}{100}\right)^{\kappa} \nabla^2 \theta \qquad (2.2.8)$$

where K_H is the horizontal kinematic eddy diffusivity coefficient.

To establish a two-level model which contains a self-determining variable static stability the thermodynamic and vorticity equations are to be applied at the same information levels, as opposed to the normal situation when the thermodynamic equation is used at one level only. Figure 2.1 shows the vertical structure of a two-level model where the isobaric surfaces 1, 2 and 3 represent the primary information levels. Therefore, with the thermodynamic equation employed at levels 1 and 3, a measure of the variable static stability at level 2 can be obtained by a vertical finite-difference representation of $\partial\theta/\partial p$ in the form

$$\left(\frac{\partial \theta_2}{\partial p}\right) \simeq \frac{\theta_3 - \theta_1}{p_3 - p_1} = 2\,\frac{\theta_3 - \theta_1}{p_s - p_T} \qquad (2.2.9)$$

From (2.2.7) it is clear that the transport of sensible heat in the vertical is a direct function of stability. Increased atmospheric instability ($\partial\theta/\partial p > \Gamma$) implies greater upward heat flow while conditions of strong stability ($\partial\theta/\partial p < \Gamma$) will create downward heat flux. In the ordinary quasi-geostrophic two-level model with the static stability

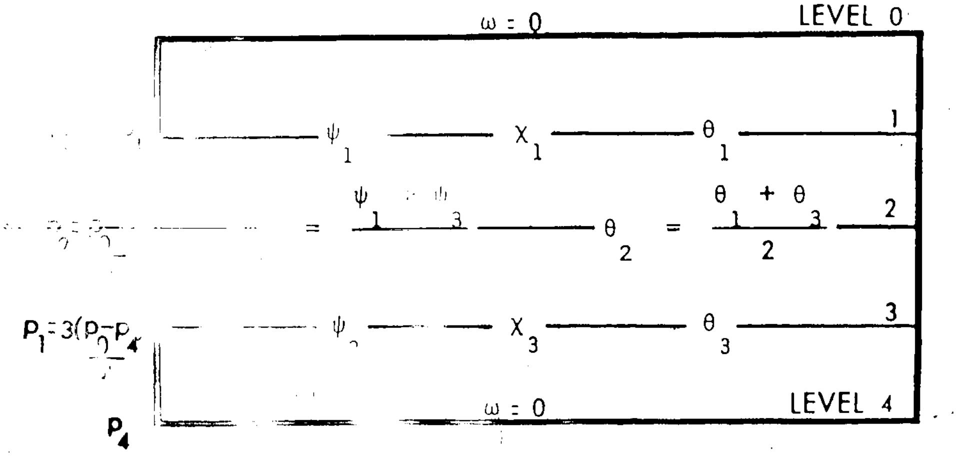

Fig. 2.1. Vertical structure of the Lorenz (1960) two-level model of the atmosphere showing the isobaric information levels. A measure of the atmospheric static stability is given by $(\theta_3 - \theta_1)/(p_3 - p_1)$.

constant it is not possible to include the effect of a variable rate of vertical heat transport. As a result diabatic heating in such models is normally input at level 2 (Figure 2.1) as a mean rate for the entire column of air extending from the surface to the top of the atmosphere. Since the whole atmosphere is essentially treated as one layer for heat input purposes the vertical diffusion terms can be ignored. Haltiner's (1967) vertical profile as given by (2.2.4) also precludes the need for vertical diffusion terms, although the profile is very dependent on the choice of a value for the constant r which has no physical interpretation.

2.3 Frictional Terms

In Chapter 1 reference was made to two studies which reported investigations of the dynamic response changes created by inserting friction into a quasi-geostrophic two-level model. However, as used by Holopainen (1961), and Haltiner and Calverly (1965), the model embodied only surface-based frictional effects. ~~In the current~~ investigation those frictional effects created by small-scale turbulent eddies in the atmospheric flow well removed from the earth's surface will also be considered.

The governing vorticity equation for the present model will be of a form similar to (2.1.14) except that a non-zero term will be inserted to account for frictional influences. Since it appears by way of the vorticity equation this frictional term will be treated as a rate of vorticity change caused by eddy momentum diffusion. If the term F_j represents the effect of friction in the model at an isobaric level j then, as with the approach employed for the sensible heating, it can be separated into two parts

$$F_j = N_j + M_j \tag{2.3.1}$$

in which N and M are the turbulent diffusion terms representing the vertical and horizontal frictional effects, respectively.

By analogy with the thermal diffusion term R, the frictional effect due to vertical momentum diffusion will be given by

$$N_j = -g \frac{\partial \tau_j}{\partial p} \qquad (2.3.2)$$

where τ_j represents the curl of the frictional stress acting on a horizontal surface and is defined as

$$\tau_j = \vec{\nabla} \times \rho K_H \left(\frac{\partial \vec{V}}{\partial z}\right)_j = -\rho^2 g K_H \frac{\partial}{\partial p} \nabla^2 \psi_j \qquad (2.3.3)$$

for which K_H is the vertical kinematic coefficient of eddy viscosity. Similarly, following closely the form given for the heating term S, the horizontal momentum diffusion term will be written as

$$M_j = \vec{\nabla} \times (K_M \nabla^2 V_j) = K_M \nabla^2 (\nabla^2 \psi_j) \qquad (2.3.4)$$

in which K_M is the horizontal kinematic coefficient of eddy viscosity.

2.4 The Model Equations

Following the vertical structure as given in Figure 2.1 the surface pressure value at the bottom of the current model is taken to be 100 kPa. The uppermost level is then given a pressure of 20 kPa as a representative value of the top of the troposphere. A common alternative is to let the upper level of the model correspond to the top of the entire atmosphere (p=0). However, for this study it will be assumed that the tropopause acts as a lid on the tropospheric motions. The remaining information levels in the model are arranged such that each is separated by a 20 kPa layer. Thus levels 1, 2 and 3 correspond to the 40, 60 and 80 kPa pressure surfaces, respectively.

The governing equations as applied at the different levels in the modelled troposphere are

$$\nabla^2\left(\frac{\partial \phi_2}{\partial p}\right) - \vec{\nabla} f \cdot \nabla\left(\frac{\partial \psi_2}{\partial p}\right) - f\nabla^2\left(\frac{\partial \psi_2}{\partial p}\right) = 0 \tag{2.4.1}$$

$$\frac{\partial \theta_j}{\partial t} + J(\psi, \theta) + \vec{\nabla}\chi \cdot \vec{\nabla}\theta_j + \omega_j\left(\frac{\partial \theta_j}{\partial p}\right) = \left(\frac{p_j}{100}\right)^{-\kappa} \frac{\dot{H}_j}{c_p} \tag{2.4.2}$$

$$\frac{\partial \psi_j}{\partial t} + J\left(\psi_j, \nabla^2\psi_j + f\right) + \vec{\nabla}\chi_j \cdot \vec{\nabla} f - f\left(\frac{\partial \omega_j}{\partial p}\right) = F_j \tag{2.4.3}$$

where j=1 or 3. Equation (2.1.15) has been differentiated with respect to pressure and applied at level 2 to form (2.4.1). The diabatic thermodynamic equation and vorticity equation (friction included) as employed at levels 1 and 3 are given by (2.4.2) and (2.4.3). The compatible form of the continuity equation remains as (2.1.12) with (2.1.11) an inherent assumption.

The equation of state for an ideal gas will also be used in the form

$$p = \rho R T \tag{2.4.4}$$

and (2.1.7) is understood to be an additional equation of state applicable to the model.

The purpose of differentiating the linear balance equation with respect to pressure is to derive a formulation which does not contain geopotential as a variable in the model. Replacement of $\partial\phi/\partial p$ using (2.1.11) and the subsequent use of (2.4.4) and (2.1.7) allows (2.4.1) to be rewritten as

$$\frac{R_p^{\kappa-1}}{100^{\kappa}}\nabla^2\theta_2 = \vec{\nabla}f\cdot\left(\vec{\nabla}\frac{\partial\psi_2}{\partial p}\right) + f\vec{\nabla}\left(\vec{\nabla}\frac{\partial\psi_2}{\partial p}\right) \qquad (2.4.5)$$

The term $\vec{\nabla}\partial\psi/\partial p$ represents the change of the rotational component of the wind with changing pressure and can be thought of as a form of vertical shear. Therefore (2.4.5) is a form of thermal wind relation for the mid-troposphere.

CHAPTER 3

NUMERICAL PROCEDURE

3.1 Boundary Conditions and Coefficient Values

If the earth's surface is assumed horizontal and the lowest level of the model remains fixed on the ground the proper lower boundary conditions are $z=0$ and $w=dz/dt=0$, where z is height. However, for convenience the conditions at the bottom of the present model will be taken to be

$$\omega = 0 \text{ and } p = p_4 = 100 \text{ kPa} \qquad (3.1.1)$$

These conditions state that the pressure at the bottom of the model remains fixed, but they do not imply a constant height field because z is not necessarily constant at the lower boundary. As will be discussed in detail later in this chapter, level 4 of the model is not always found at the sea surface. However, the variation of sea-level pressure from 100 kPa will be a perturbation quantity. Therefore, the lower boundary of the model will be treated as if it remained within a surface-based layer where the eddy stress term and the vertical heat flux are constant. No orographic variations are included in the lower boundary conditions.

At the top of the model the condition that the tropopause acts as a lid on tropospheric motions gives

$$\omega = 0 \quad \text{at} \quad p = p_0 = 20 \text{ kPa} \tag{3.1.2}$$

To prevent the diffusion of heat and momentum across the tropopause the upper boundary conditions will also necessarily include

$$h = 0 \text{ and } \tau = 0 \text{ at } p = 20 \text{ kPa} \tag{3.1.3}$$

By adopting these boundary conditions it is possible to expand the friction and heating terms more explicitly. The expression for the vertical diffusion of sensible heat (2.1.6) is evaluated at level 1 using vertical finite-differencing, to give

$$R_1 = -g\frac{h_0 - h_2}{\Delta p} = g\frac{h_2}{\Delta p} \tag{3.1.4}$$

where p represents a 40 kPa interval and h_0 is the vertical heat flux at p=0 which by (3.1.3) is zero. Using (2.2.7) to replace h_2 (3.1.4) becomes

$$R_1 = \rho^2 g^2 c_p \frac{K_v}{\Delta p}\left(\frac{\theta_3 - \theta_1}{\Delta p} - \Gamma\right) = k_h c_p\left(\theta_3 - \theta_1 - \Delta p\,\Gamma\right) \tag{3.1.5}$$

The coefficient $k_h = \rho^2 g^2 K_v / \Delta p^2$ has been introduced into (3.1.5) for simplification. The same procedure can be applied at level 3 so that

$$R_3 = -g\frac{h_2 - h_4}{\Delta p} \tag{3.1.6}$$

where the term h_2 is to be replaced as was done in (3.1.5). At the lower boundary of the model a constant surface heat flux layer has been assumed. Surface heat flux will now be defined to be

$$h_s = h_4 = \rho C_D c_p (T_g - T_a) V_s \qquad (3.1.7)$$

for which C_D is the surface drag coefficient. To convert (3.1.7) to a heating rate per unit mass in a form similar to that of (2.2.3) a constant C is introduced, where

$$C = \frac{g \rho c_p C_D}{\Delta p} \qquad (3.1.8)$$

The resulting expression for R_3 is, therefore

$$R_3 = -k_h c_p (\theta_3 - \theta_1 - \Delta p \Gamma) + C V_s (T_g - T_a) \qquad (3.1.9)$$

The entire approach as outlined above can be applied in a similar way to the vertical momentum diffusion terms. At level [illegible] pression for the friction term in the vertical using (2. [illegible] and (2.3.3) is

$$N_1 = g \frac{\tau_0 - \tau_2}{\Delta p} = -k_i \nabla^2 (\psi_1 - \psi_3) \qquad (3.1.10)$$

where the coefficient $k_i = \rho^2 g^2 K_N / \Delta p^2$ is analogous to k_h. At the lower boundary the constant stress term is defined to be

$$\tau_4 = \frac{\Delta p k_s}{g} \nabla^2 \psi_4 \qquad (3.1.11)$$

for which k_s is a constant. The term N_3 is found to be

$$N_3 = g \frac{\tau_2 - \tau_4}{\Delta p} = k_i \nabla^2 (\psi_1 - \psi_3) - k_s \nabla^2 \psi_4 \qquad (3.1.12)$$

It now remains to assign numerical values to the coefficients k_h, k_i and k_s. For the purpose of estimating these values it will be convenient to assume $K_v=K_N$ and therefore $k_i=k_h$. In unstable cases there is some basis for the argument that the magnitude of K_v is greater than K_N (Lumley and Panofsky,1964; Businger,1973). However, over a large range of stability conditions K_v and K_N have been found to be of similar magnitude. As well, the value chosen for K_v (K_N) in this study will be indicative of near-neutral stability conditions rather than of the unstable regime. Using $\partial\bar{\theta}/\partial p \simeq \Gamma$ and values suggested by Deardorff (1967) K_v is taken as being $6\text{X}10^{1}$ m²/s. A representative 60 kPa winter temperature value at mid-latitudes would be between -18°C and -25°C based on mean January temperature data (Gates,1975). Applying (2.1.7) to determine density, possible values for k_i and k_h are then $0.9\text{X}10^{-6}$ to $1.1\text{X}10^{-6}$ s^{-1}. Estimates of k_i as used in other two-level models range from $0.5\text{X}10^{-6}$ s^{-1} (Charney,1959; Kikuchi,1969) to 10^{-6} s^{-1} (Egger,1976). For this investigation $k_i=k_h=10^{-6}$ s^{-1} is used in all numerical computations.

The most commonly used value for the coefficient k_s is $4\text{X}10^{-6}$ s^{-1} as employed by Phillips (1956) and Charney (1959). Derome and Wiin-Nielson (1971) have experimented with a surface friction coefficient which was altered between $4\text{X}10^{-6}$ and $6\text{X}10^{-6}$ s^{-1}. The effect of increasing the surface friction coefficient on the behavior of their quasi-geostrophic steady-state model was relatively small. These investigators also studied the effect of having one constant surface friction coefficient over the land and a smaller constant value over the oceans. The consequence on the model predictions was only of serious import when the ratio of the two coefficients had reached a value of 6 or more. At a ratio of 2 little difference was observed over assuming one uniform friction coefficient. The earth's surface will be considered to be uniform for the purposes of this study and the imposed surface friction coefficient will be taken to be $4X10^{-6}$ s^{-1} in most calculations.

Other coefficients to be assigned numerical values are K_M and K_H. Once more, for simplification, it is presupposed that $K_M=K_H$. In assuming Fickian diffusion for the dispersion of clouds and inert tracers in the lower atmosphere, the observational evidence as suggested by Hage (1964) and Bauer (1974) would indicate that the order of magnitude of the horizontal diffusivity coefficient is 10^5-10^6 m^2/s for large-scale diffusion processes (i.e. those with a travel time of more than few days and an eddy space scale of greater than few hundred meters). Although the data refer to the horizontal dispersion of mass and may not be totally indicative of linear momentum or heat dispersion, they do provide a useful quantitative estimate of the order of magnitude which should be looked at. Phillips (1956) has employed a value of $K_M=10^5$ m^2/s in his modelling as does Kikuchi (1969). The value fixed for K_M and K_H in this study is also 10^5 m^2/s.

Surface sensible heating, as was indicated earlier, is dependent on the product of the constant C and the mean surface wind speed V_s. In order to assign a numerical value to C it is first necessary to make an estimate of the surface drag coefficient C_D. Cressman (1960) has devised a general scheme for calculating surface drag coefficients. The coefficients are evaluated using two components, the first being a dimensionless constant of $1.296 X 10^{-3}$ for all surfaces and the second is an additive quantity which is a function of the terrain roughness. Over water surfaces the total drag coefficient is resolved to be $\leq 1.3 X 10^{-3}$ while over land surfaces the variation in C_D values is $1.3 X 10^{-3}$ to $8.0 X 10^{-3}$, with the larger end of this scale reflecting very mountainous terrain. If it is assumed that $C_D = 1.3 X 10^{-3}$ for a surface wind of $V_s = 10$ m/s (i.e. measured at anemometer height) then a numerical estimate of C as calculated from (3.1.8) would be $8 X 10^{-3}$ to $9 X 10^{-3}$ J/(kg m °C). The product CV_s then compares favourably with the value of 10^{-2} J/(kg s °C) used by Haltiner (1967) to represent the same quantity. As a matter of procedure the rate of sensible heat input will be varied when analyzing the model's dynamic stability characteristics. The heating rates used will remain within a range of 0 to $2 X 10^{-2}$ J/(kg s °C).

3.2 Perturbation Equations

A useful technique for representing conditions in the mid-troposphere is to create new variables which describe the vertical mean and differential quantities across levels 1 and 3 of the model. For example, if b is any scalar quantity then the averaged or mean value of b for the layer between the two levels is given by $(b_1+b_3)/2$. Similarly the differential value would be $(b_1-b_3)/2$. If this method is applied to (2.4.2) and (2.4.3) the equations take the following forms

$$\frac{\partial\theta}{\partial t}+J(\psi,\theta)+J(\eta,\sigma)+\vec{\nabla}\chi\cdot\vec{\nabla}\sigma-\frac{\omega_2\sigma}{\Delta p}=\left(\frac{2}{5}\right)^{-\kappa}\frac{H_1}{2c_p}+\left(\frac{4}{5}\right)^{-\kappa}\frac{H_3}{2c_p} \qquad (3.2.1)$$

$$\frac{\partial\sigma}{\partial t}+J(\psi,\sigma)+J(\eta,\theta)+\vec{\nabla}\chi\cdot\vec{\nabla}\theta=\left(\frac{2}{5}\right)^{-\kappa}\frac{H_1}{2c_p}-\left(\frac{4}{5}\right)^{-\kappa}\frac{H_3}{2c_p} \qquad (3.2.2)$$

$$\frac{\partial^2\psi}{\partial t}+J(\psi,\nabla^2\psi+f)+J(\eta,\nabla^2\eta)=\frac{F_1+F_3}{2} \qquad (3.2.3)$$

$$\frac{\partial\nabla^2\eta}{\partial t}+J(\eta,\nabla^2\psi+f)+J(\psi,\nabla^2\eta)+\vec{\nabla}\chi\cdot\vec{\nabla}f-\frac{f\omega_2}{\Delta p}=\frac{F_1-F_3}{2} \qquad (3.2.4)$$

Equations (3.2.1) and (3.2.3) now represent the averaged thermodynamic and vorticity equations, respectively, while (3.2.2) and (3.2.4) are their difference counterparts. The variables as they now cccur are $\psi=(\psi_1+\psi_3)/2$, $\eta=(\psi_1-\psi_3)/2$, $\theta=(\theta_1+\theta_3)/2$, $\sigma=(\theta_1-\theta_3)/2$ and $\chi=(\chi_1-\chi_3)/2$. Vertical finite-differencing has been used for those terms involving $(\partial/\partial p)$ and it has been assumed that at any given time σ is representative of the static stability over the entire troposphere $(\theta_j=\theta_{j+1}+\sigma)$.

With the approximation that $\theta_2=(\theta_1+\theta_3)/2$ (2.4.5) as applied at level 2 becomes

$$R\,\frac{3^{\kappa-1}}{5^{\kappa}}\,\nabla^2\theta-\vec{\nabla}(f\vec{\nabla}\eta)=0 \qquad (3.2.5)$$

while the continuity equation for the model using the upper and lower boundary conditions on ω_2 can be expressed as

$$\frac{1}{2}\left[\left(\frac{\partial\omega_1}{\partial p}\right)-\left(\frac{\partial\omega_3}{\partial p}\right)\right]=\frac{\omega_2}{\Delta p}=-\nabla^2\chi \qquad (3.2.6)$$

In order to analyze the dynamics of this system a perturbation approach is used to linearize the equations. The perturbation method assumes that atmospheric motion consists of small fluctuations superimposed on a basic or steady-state flow. The fundamental premises are (Haltiner and Martin, 1957):

(a) the steady-state motion satisfies the governing equations;

(b) the overall motion (steady-state plus perturbation) also satisfies the equations; and

(c) squares (or higher orders) and products of perturbation variables appearing in the equations may be neglected in comparision with first crder terms.

For instance

$$\psi=\bar{\psi}+\psi' \qquad (3.2.7)$$

where ψ denotes the total value of the quantity, $\bar{\psi}$ is the steady-state value and ψ' refers to the perturbation value. The same representation can be applied to η, θ, σ and χ.

The steady-state flow as is suggested by its name is not a function of time. Further, it will be assumed that such flow is zonal and non-divergent in behavior. Thus, both $\bar{\chi}$ and $\bar{\omega}$ are necessarily zero. The basic state terms $\bar{\psi}$,

$\bar{\theta}$, $\bar{\eta}$ and $\bar{\sigma}$ are to be regarded as linear functions of y alone while the perturbations are to be treated as simple functions of x, y and t.

For sensible heat exchange the earth's surface is regarded as an infinite heat source (or sink) implying that its temperature field remains constant and that T_a tends to adopt to T_g. Therefore, under steady-state conditions the surface air can be assumed to be in thermal equilibrium with the underlying surface. As a result $\bar{T}_a = T_g$ and the heating rate is dependent on surface air temperature fluctuations according to

$$CV_5(T_g - T_a) = k_t(-T_a') \tag{3.2.8}$$

Variations in V_5 may be neglected since T_a' is already a perturbation quantity and so $k_t = C\bar{V}_5$.

If the potential temperature at the lower boundary of the model is linearly extrapolated from the 60 kPa level as $\theta_4 = \theta - 2\sigma$, then by assuming a sea-level pressure of 100 kPa the atmosphere-ground temperature difference is $T_a' = \theta_4' = \theta' - 2\sigma'$. This assumption is not totally valid, however, and a correction term is required to describe the possible variations in the sea-level pressure from 100 kPa.

An estimate of the pressure deviations at z=0 can be obtained by using the general form of (2.4.1) and substituting for the geopotential with $\phi = gz$. For a first approximation the term $\vec{\nabla} f \cdot \vec{\nabla}(\partial\psi/\partial p)$ is neglected and the remaining partial derivatives are replaced by finite numerical estimates giving

$$\frac{\delta z}{\delta p} \simeq \frac{f}{g}\frac{\delta \psi}{\delta p}, \tag{3.2.9}$$

where δz and $\delta\psi$ represent changes in the height and streamfunction values over some very small pressure interval δp. Perturbations in the lower boundary boundary stream function values are given by $\psi_4'=\psi'-2\eta$. Hence, assuming $\delta\psi=\psi_4'$ and using (3.2.10) the variation in the 100 kPa level height is $\delta z=f(\psi'-2\eta')/g$. Moreover, from the hydrostatic assumption (2.1.11), the change in pressure in going from 100 kPa to sea-level pressure is $\delta p=-\rho f(\psi'-2\eta')$. Figure 3.1 illustrates a situation where $\psi'-2\eta>0$ and the sea-level pressure is greater than 100 kPa.

From (2.1.7), (2.1.11) and (2.4.4) it is possible to derive the following expression for the atmospheric lapse rate

$$\frac{\partial T}{\partial z} = \left(\frac{\partial \theta}{\partial p}\frac{\partial p}{\partial z}\right)\left(\frac{p}{100}\right)^{x} - \gamma_d \tag{3.2.10}$$

in which $\gamma_d=g/c_p$ is the dry adiabatic lapse rate. Replacing the partial derivative $\partial T/\partial z$ with its finite representation $\delta T/\delta z$ and using $\partial\theta/\partial p=-2\sigma/\Delta p$ for the modelled stability parameter gives

$$\delta T = -\delta z\left[\gamma_d - \frac{2\rho g\sigma}{\Delta p}\left(\frac{p}{100}\right)^{x}\right] \tag{3.2.11}$$

where δT is now the temperature decrease in going from z=0 to the height of the model's lower boundary δz. The total variation in the surface temperature is

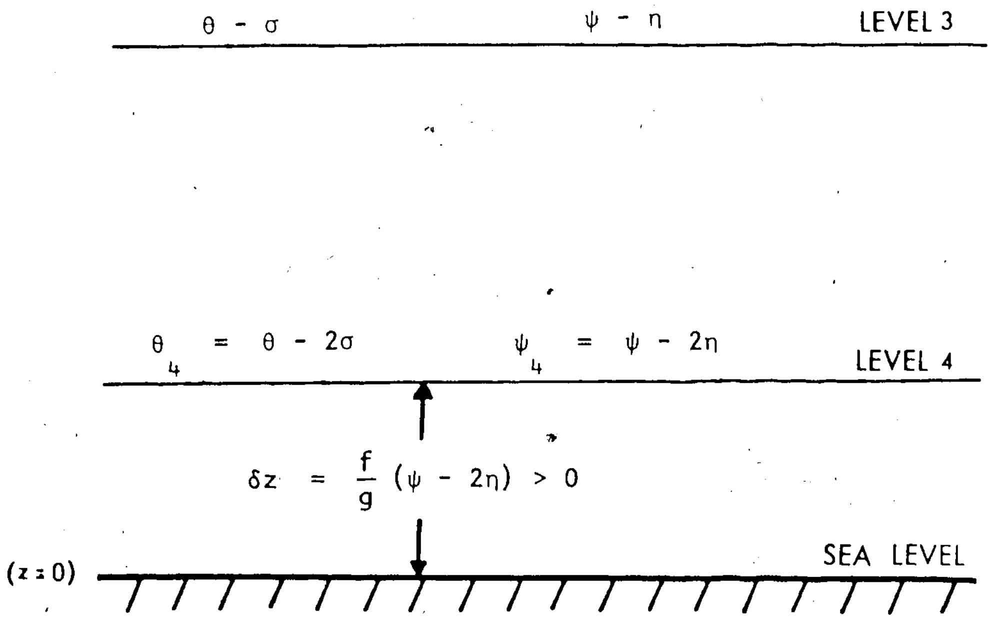

Fig. 3.1. Deviation of the sea-level pressure field from 100 kPa. Sea-level pressure values are estimated using 100 - δp (kPa), where $\delta p = -\rho g \delta z = -\rho f(\psi - 2\eta)$. The vertical cross-section shown displays a situation where the 100 kPa level is found above sea surface.

$$T_a' = \theta_4' - \delta T = (\theta' - 2\sigma') + \frac{f}{g}(\psi' - 2\eta')\left[\gamma_d - \frac{2\rho g\bar{\sigma}}{\Delta p}\left(\frac{100-\delta p}{100}\right)^{\kappa}\right] \qquad (3.2.12)$$

To a very good approximation $((100-\delta p)^{\kappa}/100) \simeq 1$ and as a result may be dropped from (3.2.13). The total surface heating rate then takes the perturbation form

$$-k_s T_a' = k_s\left[2\sigma' - \theta' - \frac{f}{g}(\psi' - 2\eta')\left(\gamma_d - \frac{2\rho g\bar{\sigma}}{\Delta p}\right)\right] \qquad (3.2.13)$$

In addition to having no surface heating under steady-state conditions, it will also be presupposed that there is no sensible heating from diffusion in the basic flow. This has already been accomplished for the horizontal diffusion term by assuming that the steady-state quantities are linear on the y-axis and constant along the x-axis. In the vertical diffusion term it is achieved by setting the countergradient $\partial\bar{\theta}/\partial p$ equal to $-2\bar{\sigma}/\Delta p$ in the model. Vertical diffusion at level 1 as expressed in (3.1.5) is then

$$R_1 = k_h c_p \left[-2\sigma - \frac{-2\bar{\sigma}}{\Delta p}\, \Delta p \right] = -2 k_h c_p \sigma' \tag{3.2.14}$$

A similar substitution can be made in (3.1.9). The value of $\bar{\sigma}$ used for the modelled atmosphere is based on January average temperature fields at 40 kPa and 80 kPa for the Northern Hemisphere (Gates, (1975)). Over the hemisphere and, in particular, over the North Pacific the mean value of the static stability is approximately 22 to 23°C for the 40 kPa layer. This would give a countergradient $\partial\bar{\theta}/\partial z$ of 4 to 5°C/km. Typically, estimates of Γ in the atmosphere vary from 0.65°C/km under clear skies to roughly 5°C/km under cloudy conditions (Deardorff, 1967).

The linearized versions of (3.2.1)-(3.2.5), after substituting for ω_2 using (3.2.6), take the form

$$\begin{aligned} \frac{\partial\theta'}{\partial t} + \frac{\partial\psi'}{\partial x}\frac{\partial\bar{\theta}}{\partial y} + U\frac{\partial\theta'}{\partial x} + \frac{\partial\eta'}{\partial x}\frac{\partial\bar{\sigma}}{\partial y} + U_T\frac{\partial\sigma'}{\partial x} + \frac{\partial\chi'}{\partial y}\frac{\partial\bar{\sigma}}{\partial y} + \bar{\sigma}\left(\frac{\partial^2\chi'}{\partial x^2} + \frac{\partial^2\chi'}{\partial y^2}\right) \\ = K_H\left(\frac{\partial^2\theta'}{\partial x^2} + \frac{\partial^2\theta'}{\partial y^2}\right) + a_2 k_h \sigma' \\ + \frac{a_3 k_t}{c_p}\left[2\sigma' - \theta' - \frac{f}{g}(\psi' - 2\eta')\left(\gamma_d - \frac{2\rho g\bar{\sigma}}{\Delta p}\right)\right] \end{aligned} \tag{3.2.15}$$

$$\frac{\partial\sigma'}{\partial t} + \frac{\partial\psi'}{\partial x}\frac{\partial\bar{\sigma}}{\partial y} + U\frac{\partial\sigma'}{\partial x} + \frac{\partial\eta'}{\partial x}\frac{\partial\bar{\theta}}{\partial y} + U_T\frac{\partial\theta'}{\partial x} + \frac{\partial\chi'}{\partial y}\frac{\partial\bar{\theta}}{\partial y}$$
$$= K_H\left(\frac{\partial^2\sigma'}{\partial x^2} + \frac{\partial^2\sigma'}{\partial y^2}\right) - a_1 k_h \sigma'$$
$$- \frac{a_3 k_t}{c_p}\left[2\sigma' - \theta' - \frac{f}{g}\left(\psi' - 2\eta'\right)\frac{\gamma_d - 2\rho g\bar{\sigma}}{\Delta p}\right] \tag{3.2.16}$$

$$\frac{\partial}{\partial t}\left(\frac{\partial^2}{\partial x^2} + \frac{\partial^2}{\partial y^2}\right)\psi' + \frac{\partial\psi'}{\partial x}\frac{\partial f}{\partial y} + U\frac{\partial^3\psi'}{\partial x^3} + U\frac{\partial^3\psi'}{\partial x\partial y} + U_T\frac{\partial^3\eta'}{\partial x^3} + U_T\frac{\partial^3\eta'}{\partial x\partial y^2}$$
$$= -\frac{k_s}{2}\left(\frac{\partial^2}{\partial x^2} + \frac{\partial^2}{\partial y^2}\right)\left(\psi' - 2\eta'\right) + K_M\left(\frac{\partial^4}{\partial x^4} + \frac{\partial^4}{\partial y^4}\right)\psi' \tag{3.2.17}$$

$$\frac{\partial}{\partial t}\left(\frac{\partial^2}{\partial x^2} + \frac{\partial^2}{\partial y^2}\right)\eta' + \frac{\partial\eta'}{\partial x}\frac{\partial f}{\partial y} + U_T\frac{\partial^3\psi'}{\partial x^3} + U_T\frac{\partial^3\psi'}{\partial x\partial y} + U\frac{\partial^3\eta'}{\partial x^3}$$
$$+ U\frac{\partial^3\eta'}{\partial x\partial y^2} + f\left(\frac{\partial^2}{\partial x^2} + \frac{\partial^2}{\partial y^2}\right)\chi' = \frac{k_s}{2}\left(\frac{\partial^2}{\partial x^2} + \frac{\partial^2}{\partial y^2}\right)\left(\psi' - 2\eta'\right)$$
$$- 2k_i\left(\frac{\partial^2}{\partial x^2} + \frac{\partial^2}{\partial y^2}\right)\eta' + K_M\left(\frac{\partial^4}{\partial x^4} + \frac{\partial^4}{\partial y^4}\right)\eta' \tag{3.2.18}$$

$$\frac{3^{\kappa-1}}{5^{\kappa}} R\left(\frac{\partial^2}{\partial x^2} + \frac{\partial^2}{\partial y^2}\right)\theta' = \left(\frac{\partial^2}{\partial x^2} + \frac{\partial^2}{\partial y^2}\right)\eta' \tag{3.2.19}$$

where $U = -\partial\bar{\psi}/\partial y$ represents the mean zonal wind and $U_T = -\partial\bar{\eta}/\partial y$ is the vertical wind shear of the basic state. The coefficients a_i $(i=1,2,3)$ are; $a_1 = (2/5)^{-\kappa} + (4/5)^{-\kappa} = 2.635$, $a_2 = (4/5)^{-\kappa} - (3/5)^{-\kappa} = -0.233$ and $a_3 = (4/5)^{-\kappa}/2 = 0.533$.

3.3 Stability Analysis

In order to investigate the stability of those perturbations in the baroclinic atmosphere depicted by the model, harmonic-wave solutions of the following form are assumed

$$\psi' = \hat{\psi}(y)\exp[im(x-ct)] \qquad \eta' = \hat{\eta}(y)\exp[im(x-ct)]$$

$$\theta' = \hat{\theta}(y)\exp[im(x-ct)] \qquad \sigma' = \hat{\sigma}(y)\exp[im(x-ct)] \tag{3.3.1}$$

$$\chi' = \hat{\chi}(y)\exp[im(x-ct)]$$

where $m=2\pi/L_y$ is the wavenumber and L_x is the wavelength on the x-axis, c is the phase velocity of the wave, $\sqrt{i}= -1$, and $\hat{\psi}(y)$, $\hat{\eta}(y)$, $\hat{\theta}(y)$, $\hat{\sigma}(y)$ and $\hat{\chi}(y)$ are the wave amplitudes. The latitudinal dependence of the perturbations enters through the amplitudes which will be given a simple meridional variation

$$\hat{\psi}(y) = \hat{\psi}\cos(ny) \tag{3.3.2}$$

where $n=2\pi/L_y$ is the wavenumber and L_y is the wavelength in the y-direction. Substitution of these solutions into (3.2.16)-(3.2.20) leads to a set of homogeneous equations which can be represented in matrix form as

$$[B][A]=0 \tag{3.3.3}$$

Here [A] is the amplitude matrix

$$\begin{bmatrix} \hat{\psi} \\ \hat{\eta} \\ \hat{\theta} \\ \hat{\sigma} \\ \hat{\chi} \end{bmatrix}$$

and [B] is the coefficient matrix defined as

$$\begin{bmatrix} (C-U)+b^1 & b^2 & 0 & 0 & 0 \\ b^3 & (C-U)+b^4 & 0 & 0 & b^5 \\ b^6 & b^7 & -(C-U)+b^8 & b^9 & b^{10} \\ b^{11} & b^{12} & b^{13} & -(C-U)+b^{14} & b^{15} \\ 0 & b^{16} & b^{17} & 0 & 0 \end{bmatrix}$$

where

$b^1 = \frac{\beta}{m^2+n^2} + \frac{ik_s}{2m} + \frac{iK_M(m^4+n^4)}{m(m^2+n^2)}$

$b^2 = -U_T - \frac{ik_s}{m}$

$b^3 = -U_T - \frac{ik_s}{2m}$

$b^4 = \frac{\beta}{m^2+n^2} + \frac{i(k_s+2k_i)}{m} + \frac{iK_M(m^4+n^4)}{m(m^2+n^2)}$

$b^5 = \frac{if}{m}$

$b^6 = -\frac{5^{\kappa}}{3^{\kappa}}\frac{fU_T}{R} - \frac{ia_3k_tfG}{gc_pm}$

$b^7 = \frac{5^{\kappa}}{3^{\kappa}}(1-\kappa)\frac{fU_T}{R} + \frac{i2a_3k_tfG}{gc_pm}$

$b^8 = \frac{i(m^2+n^2)K_H}{m} - \frac{ia_3k_t}{mc_p}$

$b^9 = U_T + \frac{i2a_2k_t}{mc_p} + \frac{ia_3k_h}{m}$

$b^{10} = \frac{i5^{\kappa}fU_Tn\tan(ny)}{3^{\kappa}Rm} + \frac{i(m^2+n^2)}{m}\sigma_0$

$b^{11} = \frac{5^{\kappa}(1-\kappa)fU_T}{3^{\kappa}R} + \frac{a_3k_tfG}{gc_pm}$

$b^{12} = -\frac{5^{\kappa}fU_T}{3^{\kappa-1}R} - \frac{i2a_3k_tfG}{gc_pm}$

$b^{13} = U_T + \frac{ia_3k_t}{mc_p}$

$b^{14} = -\frac{i(m^2+n^2)K_H}{m} - \frac{i2a_3k_t}{mc_p} - \frac{ia_2k_h}{m}$

$b^{15} = -\frac{i5^{\kappa}fU_Tn}{3^{\kappa-1}Rm}\tan(ny)$

$b^{16} = -f$

$$b_{17} = \frac{3^{\kappa-1}}{5^{\kappa}} . R$$

In the coefficients $G=(\gamma_d - 2\rho g\bar{\sigma}/\Delta p)$ and $\beta=\partial f/\partial y$ is the meridional derivative of the Coriolis parameter. Use has also been made of the following relations

$$\frac{\partial\bar{\theta}}{\partial y} = \frac{-5^{\kappa} f U_T}{3^{\kappa-1} R} \qquad (3.3.4)$$

$$\frac{\partial\bar{\sigma}}{\partial y} = (1-\kappa)\frac{5^{\kappa} f U_T}{3^{\kappa} R} \qquad (3.3.5)$$

which were found by assuming a constant U_T in the mid-troposphere and then requiring the zonal flow to satisfy (3.2.20).

A necessary and sufficient condition that (3.3.3) has a non-trivial solution is that the determinant of [B] be zero. Expansion of the determinant and grouping of the terms in decreasing orders of (c-U) gives a cubic frequency equation which can be solved for a variety of wavenumbers, surface heating rates and steady-state quantities.

The phase velocities which are obtained in the solutions to this cubic frequency equation are typically complex values, $c=c_R+ic_I$, in which c_R represents the real portion and c_I the imaginary portion of the wave phase velocity. A perturbation wave is, therefore, of the form

$$\psi' = \hat{\psi}\cos(ny)\exp(mc_I t)\exp(im(x-c_R t)) \qquad (3.3.6)$$

Such a waveform propagates in the west-east direction at a speed c_R with a time-dependent numerical amplification (or damping) factor of $\exp(mc_I t)$. More specifically it is the value of c_I which determines the stability condition of the wave. The stability classifications are given in Table 1.

Table 1. Stability conditions for the harmonic waveforms as a function of the imaginary portion of the phase velocity.

STABILITY CLASSIFICATION		
UNSTABLE:	$c_I < 0$,	amplifying wave with time
NEUTRAL:	$c_I = 0$,	waveform unchanging
STABLE:	$c_I > 0$,	damped wave with time

The rate of amplification of an unstable wave is dependent on the exponent mc_I. A useful way of representing this growth rate is by a quantity known as the e-folding time (t_e) which is defined by

$$t_e = \frac{1}{mc_I} = \frac{L_x}{2\pi c_I} \tag{3.3.7}$$

The value of t_e is the time required for an unstable wave to increase in amplitude by a factor of e=2.71828. The implication of a small e-folding time is that the waveform is very unstable and amplifying rapidly.

3.4 Wave Dynamics

When studying the phase and amplitude characteristics of the perturbations it is useful to express the harmonic solutions in a somewhat different form. Corresponding to each value of the phase velocity c_k (k=1,2,3) as given by the frequency equation, the system of equations represented by (3.3.3) can be solved for values of $\hat{\psi}_k$, $\hat{\eta}_k$, $\hat{\theta}_k$, $\hat{\sigma}_k$ and $\hat{\chi}_k$ if initial conditions for each perturbation wave are specified. The procedure is then to write the general perturbation waveforms as sums of components

$$
\begin{aligned}
\psi' &= \sum_{k=1}^{3} \hat{\psi}_k \cos(ny) \exp im(x-c_k t) \\
\eta' &= \sum_{k=1}^{3} \hat{\eta}_k \cos(ny) \exp im(x-c_k t) \\
\theta' &= \sum_{k=1}^{3} \hat{\theta}_k \cos(ny) \exp im(x-c_k t) \\
\sigma' &= \sum_{k=1}^{3} \hat{\sigma}_k \cos(ny) \exp im(x-c_k t) \\
\chi' &= \sum_{k=1}^{3} \hat{\chi}_k \cos(ny) \exp im(x-c_k t)
\end{aligned}
\qquad (3.4.1)
$$

It is convenient to substitute for the terms $\hat{\eta}_k$ and $\hat{\chi}_k$ from (3.3.3) using

$$\hat{\eta}_k = \frac{-b^{17}}{b^{16}} \hat{\theta}_k \qquad (3.4.2)$$

$$\hat{\chi}_k = \frac{-b^3}{b^5} \hat{\psi}_k + \left(\frac{c_k - U}{b^5} + b^4 \right) \frac{b^{17}}{b^{16}} \hat{\theta}_k \qquad (3.4.3)$$

The reduced system of equations in terms of $\hat{\psi}_k$, $\hat{\theta}_k$ and $\hat{\sigma}_k$ is

$$[D][E]=0 \qquad (3.4.4)$$

where $[E]=\begin{bmatrix}\hat{\psi}_k\\ \hat{\theta}_k\\ \hat{\sigma}_k\end{bmatrix}$, and $[D]=\begin{bmatrix} d_k^1 & d_k^2 & 0\\ d_k^3 & d_k^4 & d_k^5\\ d_k^6 & d_k^7 & d_k^8\end{bmatrix}$.

The coefficients d_k^j $(j=1,2,\ldots,8\ k=1,2,3)$ are

$d_k^1= (c_k-U)+b^1$

$d_k^5= b^9$

$d_k^2= -\dfrac{b^2 b^{17}}{b^{16}}$

$d_k^6= b^{11}-\dfrac{b^3 b^{15}}{b^5}$

$d_k^3= b^6-\dfrac{b^3 b^{10}}{b^5}$

$d_k^7= b^3-\dfrac{b^{17}}{b^{16}}\left(b^{12}+b^{15}\left[\dfrac{c_k-U+b^{14}}{b^5}\right]\right)$

$d_k^4=(c_k-U)+b^8-\dfrac{b^{17}}{b^{16}}\left[b^7-b^{10}\,\dfrac{c_k-U+b^4}{b^5}\right]$

$d_k^8= -(c_k-U)+b^{14}$

The initial conditions specified at t=0 in the solutions to (3.4.4) are of the type

$$\psi'(t=0)=\hat{\psi}_0\cos(ny)\exp(imx)$$

$$\theta'(t=0)=\hat{\theta}_0\cos(ny)\exp(im\ +\varepsilon_\theta) \qquad (3.4.5)$$

$$\sigma'(t=0)=\hat{\sigma}_0\cos(ny)\exp(imx+\varepsilon_\sigma)$$

in which $\hat{\psi}_0$, $\hat{\theta}_0$ and $\hat{\sigma}_0$ are the initial amplitude values and ε_θ and ε_σ are the initial phase angles of θ' and σ' with respect to ψ'. For example, $\varepsilon_\theta < 0$ implies that the potential temperature wave initially lags the stream function, while $\varepsilon_\theta > 0$ means that the potential temperature wave leads. If $\varepsilon_\theta = 0$ the two waves are initially in phase.

It follows from (3.4.1) and (3.4.5) that

$$\begin{aligned} \sum_{k=1}^{3} \hat{\psi}_k &= \hat{\psi}_0 \\ \sum_{k=1}^{3} \hat{\theta}_k &= \hat{\theta}_0 \exp(i\varepsilon_\theta) \\ \sum_{k=1}^{3} \hat{\sigma}_k &= \hat{\sigma}_0 \exp(i\varepsilon_\sigma) \end{aligned} \tag{3.4.6}$$

Furthermore, from (3.4.4) $\hat{\theta}_k$ and $\hat{\sigma}_k$ can be expressed in terms of $\hat{\psi}_k$ as

$$\begin{aligned} \sum_{k=1}^{3} \hat{\theta}_k &= \sum_{k=1}^{3} r_k \hat{\psi}_k \\ \sum_{k=1}^{3} \hat{\sigma}_k &= \sum_{k=1}^{3} s_k \hat{\psi}_k \end{aligned} \tag{3.4.7}$$

where $r_k = -d^1_k / d^2_k$ and $s_k = -d^6_k / d^8_k + d^7_k\, d^1_k / (d^8_k\, d^2_k)$. From (3.4.6) and (3.4.7) the following general solutions for $\hat{\psi}_1$, $\hat{\psi}_2$ and $\hat{\psi}_3$ may be obtained

$$\begin{aligned} \hat{\psi}_1 &= -\hat{\psi}_2 - \hat{\psi}_3 + \hat{\psi}_0 \\ \hat{\psi}_2 &= \frac{\sigma_0 e^{i\varepsilon_\sigma} - s_1 \hat{\psi}_0 + (s_1 - s_3)\hat{\psi}_3}{s_2 - s_1} \\ \hat{\psi}_3 &= \frac{\hat{\theta}_0 e^{i\varepsilon_\theta} + (r_1 - r_2)\left(\frac{\hat{\sigma} e^{i\varepsilon_\sigma} - s_1 \hat{\psi}_0}{s_2 - s_1}\right) - r_1 \hat{\psi}_0}{-(r_1 - r_2)\left(\frac{s_1 - s_3}{s_2 - s_1}\right) - r_1 + r_3} \end{aligned} \tag{3.4.8}$$

Knowing the initial amplitude and phase values, the phase velocity c_k and parameters such as U, f, U_T, $\bar{\sigma}$ and others it is possible to determine $\hat{\psi}_3$ and then, in succession, the values of $\hat{\psi}_2$, $\hat{\psi}_1$, $\hat{\theta}_k$, $\hat{\sigma}_k$ and $\hat{\omega}_k$ with the component amplitudes for the vertical velocity determined from using the model's continuity equation and the velocity potential values $\hat{\chi}_k$. It is also useful to derive wave components representing surface sensible heating ($\hat{h}_k$) from the existing waveforms by employing (3.2.14).

Although each perturbation is written as a sum of three components, a single wave representation can be made which has its amplitude and phase angle as functions of time From (3.4.1) and by writing the phase velocities and amplitudes in their complex form the mean perturbation stream function may be expressed as

$$\psi' = \sum_{k=1}^{3} \left(\hat{\psi}_{k_R} + i\hat{\psi}_{k_I}\right) \cos(ny) \exp\left[mc_{k_I} t + im\left(x - c_{k_R} t\right)\right] \qquad (3.4.9)$$

In complex polar coordinates this is equivalent to

$$\psi' = \sum_{k=1}^{3} \left|\hat{\psi}_k\right| \cos(ny)\, e^{mc_{k_I} t}\, e^{i(q_k - mc_{k_R} t)}\, e^{imx} \qquad (3.4.10)$$

in which $|\hat{\psi}_k| = (\hat{\psi}_{k_R}^2 + i\hat{\psi}_{k_I}^2)^{1/2}$ represents the modulus of the complex vector $\hat{\psi}_{k_R} + i\hat{\psi}_{k_I}$ and $q = \arctan(\hat{\psi}_{k_I} / \hat{\psi}_{k_R})$ is the vector angle from the positive real axis. Combining the modulus and amplification factor into one term $\hat{\psi}_k^* = |\hat{\psi}_k| \exp(mc_{kI} t)$ and defining $q_k^* = q_k - mc_{kR} t$ allows (3.4.10) to be rewritten as a single wave solution of the type

$$\psi' = \hat{\psi}_A \cos(ny) e^{i\psi_p} e^{imx} \qquad (3.4.11)$$

where the amplitude $\hat{\psi}_A$ is

$$\hat{\psi}_A = \left[\left(\sum_{k=1}^{3} \hat{\psi}_k^* e^{iq_k^*} \right)_R^2 + \left(\sum_{k=1}^{3} \hat{\psi}_k^* e^{iq_k^*} \right)_I^2 \right]^{1/2}$$

$$= \left[\left(\sum_{k=1}^{3} \hat{\psi}_k^* \cos q_k^* \right)^2 + \left(\sum_{k=1}^{3} \hat{\psi}_k^* \sin q_k^* \right)^2 \right]^{1/2} \qquad (3.4.12)$$

and the phase angle ψ_p is determined from

$$\psi_p = \arctan \frac{\left(\sum_{k=1}^{3} \hat{\psi}_k^* e^{iq_k^*} \right)_I}{\left(\sum_{k=1}^{3} \hat{\psi}_k^* e^{iq_k^*} \right)_R}$$

$$= \arctan \frac{\sum_{k=1}^{3} \hat{\psi}_k^* \sin q_k^*}{\sum_{k=1}^{3} \hat{\psi}_k^* \cos q_k^*} \qquad (3.4.13)$$

In the same manner the remaining perturbation quantities θ', σ', ω', h' and η' may be described in a form similar to that of (3.4.12) with their respective amplitudes $\hat{\theta}_A$, $\hat{\sigma}_A$, $\hat{\omega}_A$, $\hat{h}_A$, $\hat{\eta}_A$ and phase angles θ_p, σ_p, ω_p, h_p, η_p. Calculations were carried out to determine these values as functions of time and for varying initial conditions as well as for different basic flow properties.

CHAPTER 4

NUMERICAL RESULTS AND DISCUSSION

4.1 Preliminary Comments

The present model, like that of Haltiner (1967) incorporates a surface sensible heat flux but, unlike the latter, it also allows for the inclusion of surface friction effects, heat and momentum diffusion terms and a simple meridional variation in the perturbation field. The numerical investigations of the dynamic response characteristics of the model for different states of current flow are discussed first. These flow regimes are indentified in the following manner:

(i) Model 1. Adiabatic flow with no frictional vorticity terms included.

(ii) Model 2. Sensible heating (including the redistribution of heat by thermal diffusivity) with no frictional vorticity terms.

(iii) Model 3. Adiabatic flow with frictional vorticity terms included.

(iv) Model 4. Sensible heating with frictional vorticity terms included.

As an initial simplification it is assumed in each of the four 'models' that the perturbation field is not a function of latitude. Later, a latitudinal dependence is incorporated in conjunction with model 4 and the calculations are redone. This particular version of the modelling is simply referred to as the 'full model'.

The latter part of this chapter focusses on the behavior of the longest waves. Of specific interest are those features of long waves which can be applied to blocking ridge development in the North Pacific.

4.2 Influence of Sensible Heating and Friction on Dynamic Stability Response

In order to compare the various model runs the steady-state atmospheric quantities were held constant unless otherwise noted with $U_T=10$ m/s, $f(45N)=1.0312X10^{-4}$ s^{-1}, $\beta(45N)=1.61X10^{-11}$ $m^{-1}s^{-1}$ and $\bar{\sigma}=12°C$. The phase velocity solutions of models 1 through 4 were then obtained from the corresponding cubic frequency equation. Since the frequency equation is solved in terms of (c_k-U) it should be kept in mind that the real portion of any solution represents the phase velocity of the perturbation wave relative to the speed of the mean westerly wind.

Figures 4.1a and 4.1b show both the imaginary and real portions of the solutions (c_k-U) as a function of wavelength L_x for models 1 and 2, respectively. Each case exhibits a neutral or near-neutral solution $(c_I \simeq 0)$ arbitrarily denoted I1, a damped solution $(c_I<0)$ designated curve I2 and an unstable solution I3 $(c_I>0)$. The corresponding real parts to these curves are shown as R1, R2 and R3.

Features apparent in the adiabatic-frictionless

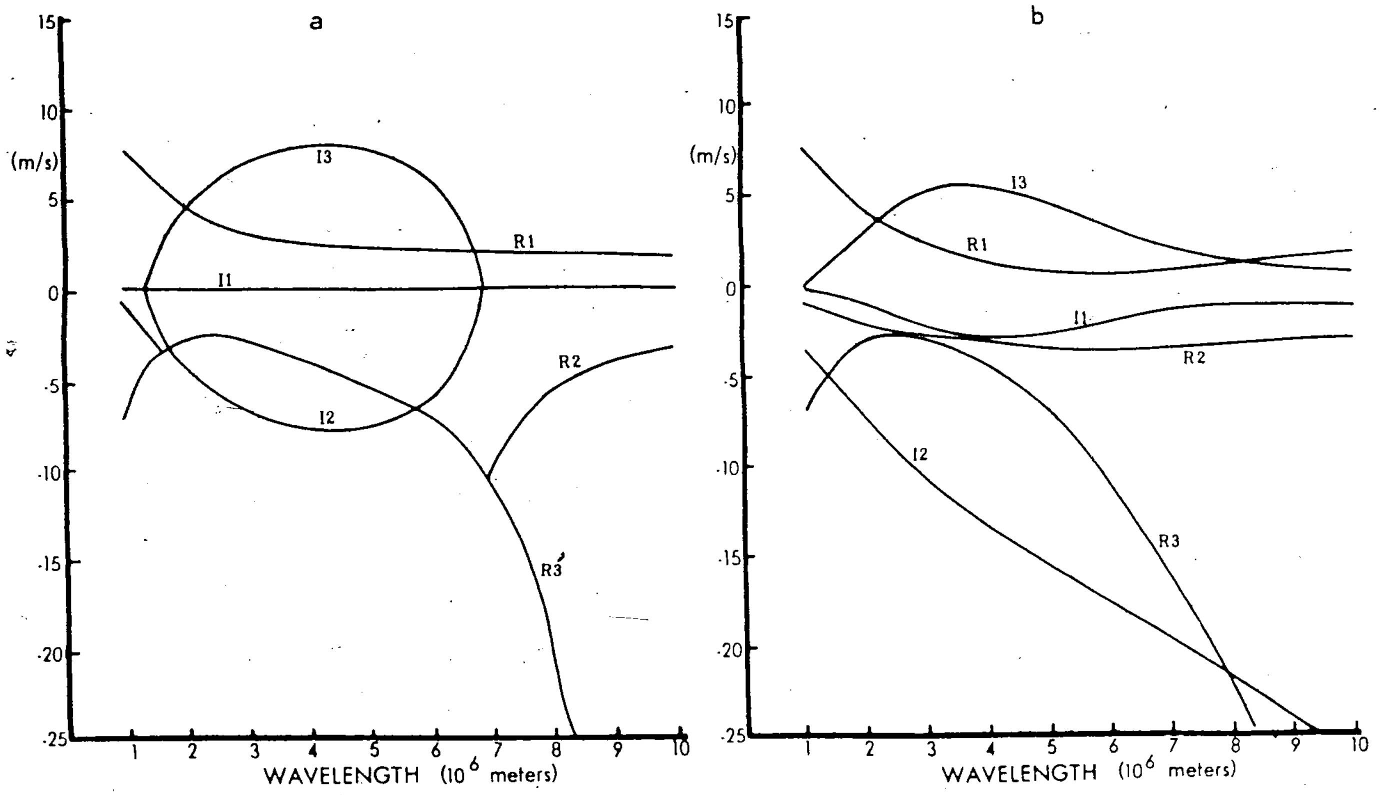

Fig. 4.1. Response curves for (a) adiabatic-frictionless flow (model 1), and (b) diabatic-frictionless flow (model 2). Phase velocities (ordinate) are in meters per second with curves R_1, R_2 and R_3 the real parts and I_1, I_2 and I_3 the imaginary parts of the frequency equation solutions ($c_k' - U$), k = 1,2,3. Wavelengths (abscissa) are in units of 1000 km in the east-west direction.

Table [illegible]2. Real (R3) and imaginary (I3) portions of the phase velocities over the unstable waveband of Fig. 4.1a and the corresponding e-folding times (t_e).

Wavelength (km)	R3 (m/s)	I3 (m/s)	t_e (days)
1000	-7.20	0.00	
1500	-3.29	2.05	1.35
2000	-2.80	4.50	0.82
2500	-2.73	5.99	0.77
3000	-3.00	6.95	0.80
3500	-3.49	7.53	0.86
4000	-4.14	7.82	0.94
4500	-4.93	7.86	1.06
5000	-5.83	7.66	1.20
5500	-6.86	7.16	1.42
6000	-7.99	6.27	1.76
6500	-9.23	4.74	2.52
7000	-11.01	0.00	

solutions of Fig. 4.1a are that the unstable and damped waves propagated at the same speeds over the entire range of unstable wavelengths. Furthermore, these speeds were always slower than that of the mean westerly wind speed. The neutral wave in turn always travelled faster than the zonal wind speed as indicated by the R1 curve being positive at all wavelengths.

Introduction of sensible heating to the model as shown in Fig. 4.1b has diminished the amplitude of the I3 curve at

Table 3. Real (R3) and imaginary (I3) portions of the phase velocities over the unstable waveband of Fig. 4.1b and the corresponding e-folding times (t_e)

Wavelength (km)	R3 (m/s)	I3 (m/s)	t_e (days)
1000	-7.[illegible]7	0.06	30.70
1500	-4.59	1.13	2.45
2000	-3.07	2.81	1.31
2500	-2.55	4.20	1.10
3000	-2.72	5.07	1.09
3500	-3.27	5.47	1.18
4000	-4.09	5.50	1.34
4500	-5.18	5.22	1.59
5000	-6.61	4.67	1.97
5500	-8.47	3.93	2.58
6000	-10.82	3.17	3.49
6500	-13.57	2.54	4.71
7000	-16.60	2.06	6.26
7500	-19.85	1.70	8.13
8000	-23.28	1.42	10.38
8500	-26.90	1.21	12.94
9000	-30.69	1.05	15.79
9500	-34.66	0.91	19.23
10000	-38.82	0.81	22.74
10500	-43.15	0.72	26.86
11000	-47.68	0.64	31.66
11500	-52.39	0.58	36.52
12000	-57.30	0.53	41.71

lower and intermediate wavelengths, but at the same time has extended the band of unstable wavelengths to beyond 10,000 km. Other changes from the values of model 1 are that the I2 curve now shows much stronger damping at longer wavelengths and the R2 and R3 curves no longer coincide over any interval. The coefficient for surface heating in this case was chosen as $k_t = 10^{-2}$ J/(kg s °C) and, unless otherwise noted, this value was used in all calculations where heating was incorporated.

Haltiner's (1967) findings using the same value of surface heating and a vertical wind shear of 10 m/s over a 25 kPa layer show qualitatively the same shape as the curves of Fig. 4.1b. Tables 2 and 3 give the values for the unstable waveband at every 500 km for models 1 and 2 from the present study, while Haltiner's results are found in Table 4. The latter two tables are quite comparable over wavelengths from 3500 to 8000 km. Outside of this range the present model gave a slightly more unstable wave as indicated by the c_I values and the computed e-folding times.

The results of incorporating friction are presented in Fig. 4.2a. It is apparent that there are two regions at the extremes of the unstable waveband where increased instability occurred when compared with that of the adiabatic-frictionless case. The amount of broadening of the [illegible] at longer wavelengths was very small, however, when [illegible] with Fig. 4.1b. It is also evident by compa[illegible] of Tables 2 and 5 that, except within these two

Table 4. Real (R3) and imaginary (I3) portions of the phase velocities over the unstable waveband of Haltiner (1967) for sensible heating with no friction. ($k_h = 10^{-2}$ J/(kg s ^{o}C), r = 2, U_T = 10 m/s and $\bar{\sigma}$ = 15°C over a 25 kPa layer)

Wavelength (km)	R3 (m/s)	I3 (m/s)	t_e (days)
1000	-8.39	0.00	
1500	-6.31	0.24	11.51
2000	-4.45	2.06	1.79
2500	-4.03	3.49	1.32
3000	-4.06	4.44	1.24
3500	-4.44	5.03	1.28
4000	-5.12	5.30	1.39
4500	-6.07	5.30	1.56
5000	-7.30	5.04	1.83
5500	-8.85	4.55	2.28
6000	-10.80	3.88	2.85
6500	-13.19	3.10	3.86
7000	-16.04	2.37	5.44
7500	-19.27	1.78	7.76
8000	-22.76	1.36	10.84
8500	-26.45	1.06	14.77
9000	-30.31	0.85	19.50
9500	-34.34	0.69	25.36
10000	-38.54	0.58	31.76
10500	-42.92	0.49	39.47
11000	-47.47	0.42	48.24
11500	-52.21	0.36	58.84
12000	-57.14	0.31	71.31

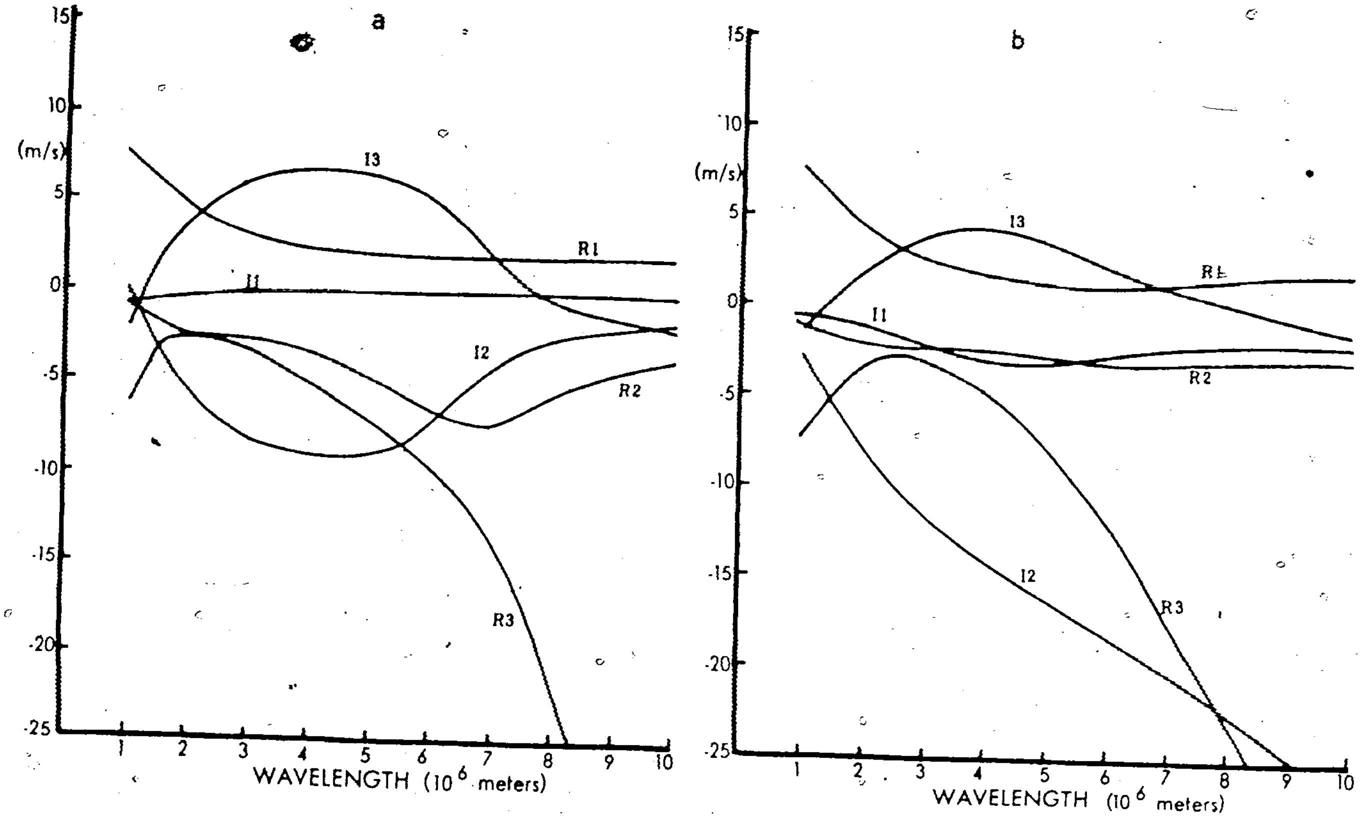

Fig. 4.2. Response curves for (a) adiabatic flow with friction included (model 3), and (b) conditions of diabatic heating with friction included (model 4). Phase velocities (ordinate) are in meters per second with curves R_1, R_2 and R_3 the real parts and I_1, I_2 and I_3 the imaginary parts of the frequency equation solutions $(c_k - U)$, $k = 1,2,3$. Wavelengths (abscissa) are in units of 1000 km in the east-west direction.

rrow regions, the amplitude of the I3 curve has everywhere been reduced.

Table 5. Real (R3) and imaginary (I3) portions of the phase velocities over the unstable waveband of Fig. 4.2a and the corresponding e-folding times (t_e).

Wavelength (km)	R3 (m/s)	I3 (m/s)	t_e (days)
1000	-1.60	-8.23	
1500	-2.66	1.45	1.91
2000	-2.82	3.68	1.00
2500	-3.03	5.11	0.90
3000	-3.50	6.04	0.92
3500	-4.17	6.59	0.98
4000	-4.98	6.86	1.07
4500	-5.92	6.88	1.21
5000	-6.98	6.65	1.39
5500	-8.18	6.15	1.65
6000	-9.54	5.29	2.09
6500	-11.19	3.93	3.05
7000	-13.66	1.91	6.75
7500	-17.55	0.28	49.34
8000	-21.63	<0	

The response curves of model 4 containing both sensible heating and friction are given in Fig. 4.2b. A longwave cutoff is now found near 8500 km, roughly 1500 km longer than the cutoff shown for adiabatic-frictionless conditions. It is also significant that over the unstable waveband the

R3 values of Fig. 4.2b imply much lower propagation rates than found initially in Fig. 4.1a. For instance, a mean wind of U=15 m/s would mean that every unstable wave in model 1 would propagate eastward as it amplified. With the inclusion of both sensible heating and friction this value for the mean wind would result in a stationary unstable wave of about 6000 km (Table 6) while at longer wavelengths

Table 6. Real (R3) and imaginary (I3) portions of the phase velocities over the unstable wave band of Fig. 4.2b and the corresponding e-folding times (t_e).

Wavelength (km)	R3 (m/s)	I3 (m/s)	t_e (days)
1500	-3.11	<0	
2000	-2.81	1.70	2.17
2500	-3.17	3.08	1.50
3000	-3.89	3.94	1.40
3500	-4.89	4.31	1.50
4000	-6.14	4.33	1.70
4500	-7.71	4.06	2.04
5000	-9.63	3.56	2.59
5500	-11.92	2.93	3.46
6000	-14.53	2.25	4.91
6500	-17.43	1.61	7.44
7000	-20.56	1.04	12.40
7500	-23.91	0.54	25.59
8000	-27.45	0.10	147.37
8500	-31.19	<0	

unstable wave growth could occur as the wave retrogressed westwards. The implications of this will be investigated further in the discussion on blocking ridge development.

The rate of surface sensible heat exchange and the degree of surface friction have as yet been held constant. Figure 4.3 illustrates the change in the unstable curve for model [illegible] under various rates of surface heating. The basic flow parameters were unchanged from the values used earlier. It is seen that increasing the surface heat input resulted in a further reduction of the curve amplitude at lower and intermediate wavelengths. Conversely the region at longer wavelengths exhibited increased instability. It is also noticeable that the region of enhanced instability between successive increments in the value of k_t was gradually shifted to longer wavelengths, indicating that further increases in the heating rate would result in greater instability at extremely long waves only.

Increasing the degree of surface friction through the coefficient k_s in model 3 resulted in only marginal increases in the amount of instability at the edges of the unstable waveband. However, in changing k_s from $4X10^{-6}$ to 10^{-5} s^{-1} a fairly significant reduction in the amplitude of the I3 curve did occur at intermediate values of the wavelength range.

4.3 Variation of the Steady-state Flow Parameters

The response values of the perturbation field are

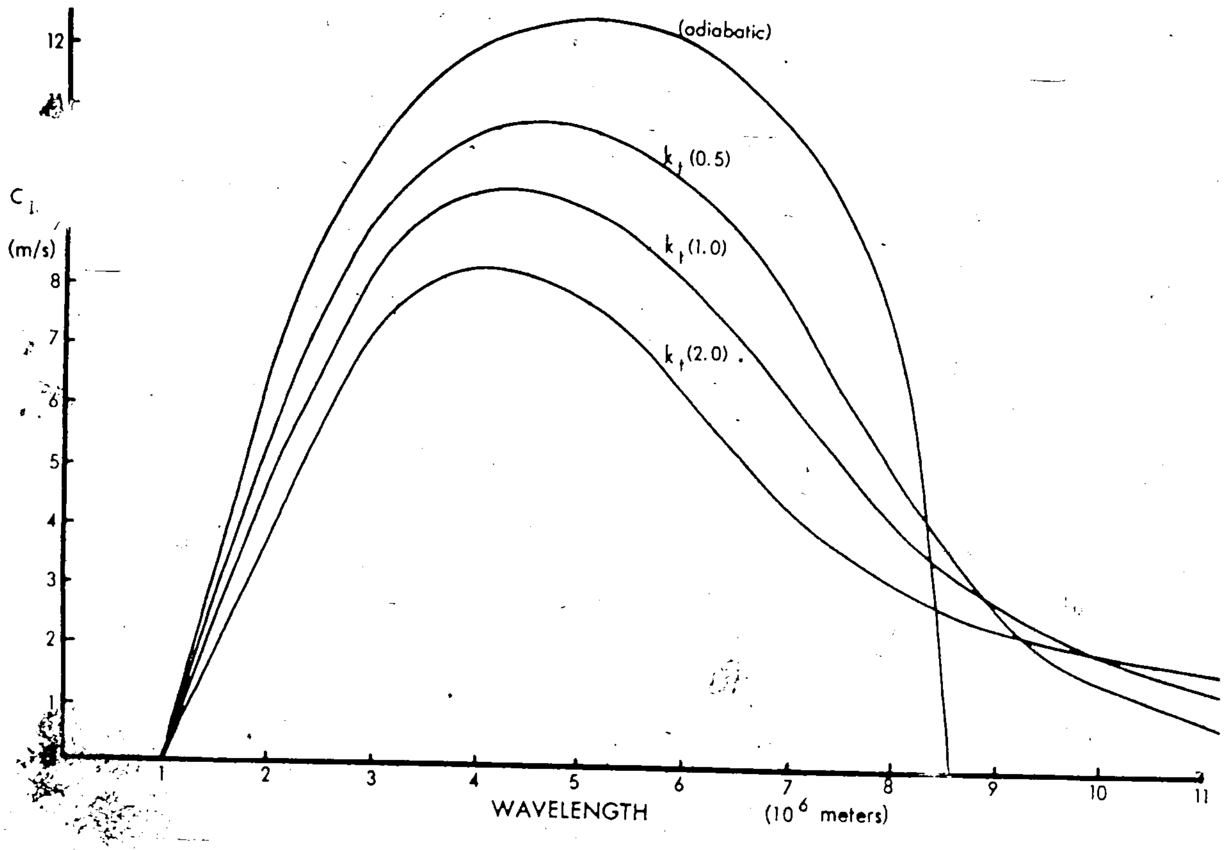

Fig. 4.3. Response of the stability curve c_{I3} to different surface sensible heating rates. The diabatic curves, taken from model 2, are labelled with the value of the surface sensible heating coefficient k_t (10^{-2} J/(kg s ^{o}C)) used in the calculations. The adiabatic curve is from model 1.

affected if certain properties of the steady-state flow change. This is easily seen in the case of a change in the zonal wind U. Since U appears as part of the real portion of the frequency equation solution it does not influence the stability of the waves. Its main influence is to define the 'absolute' speed of the waves on the x-axis and a change in U results in a corresponding shift of these values. This is important because the value assigned to U will play a major role in determining whether it is possible to have a stationary wave within the unstable band of wavelengths.

The mean vertical wind shear U_T is a measure of the baroclinicity of the basic state and the numerical results indicated that the greater the shear the greater the possible instablity of the perturbations in the flow. The solid curves of Fig. 4.4 represent the change in stability experienced in model 4 under the same conditions as employed earlier except that U_T was varied. With greater wind shear the instability of the I3 curve was increased at all wavelengths. The effect on the real portion of the unstable solution was to decrease the speed of the waves by a few meters per second. In general very little instability was observed in any of the model types at wavelengths greater than 6000 km until the wind shear had exceeded 5-6 m/s. Thus, at low mid-tropospheric wind shear values the possibility of longwave instability is small.

Figure 4.4 also shows the effect on the I3 curve of changing the mean static stability. As the mean stability

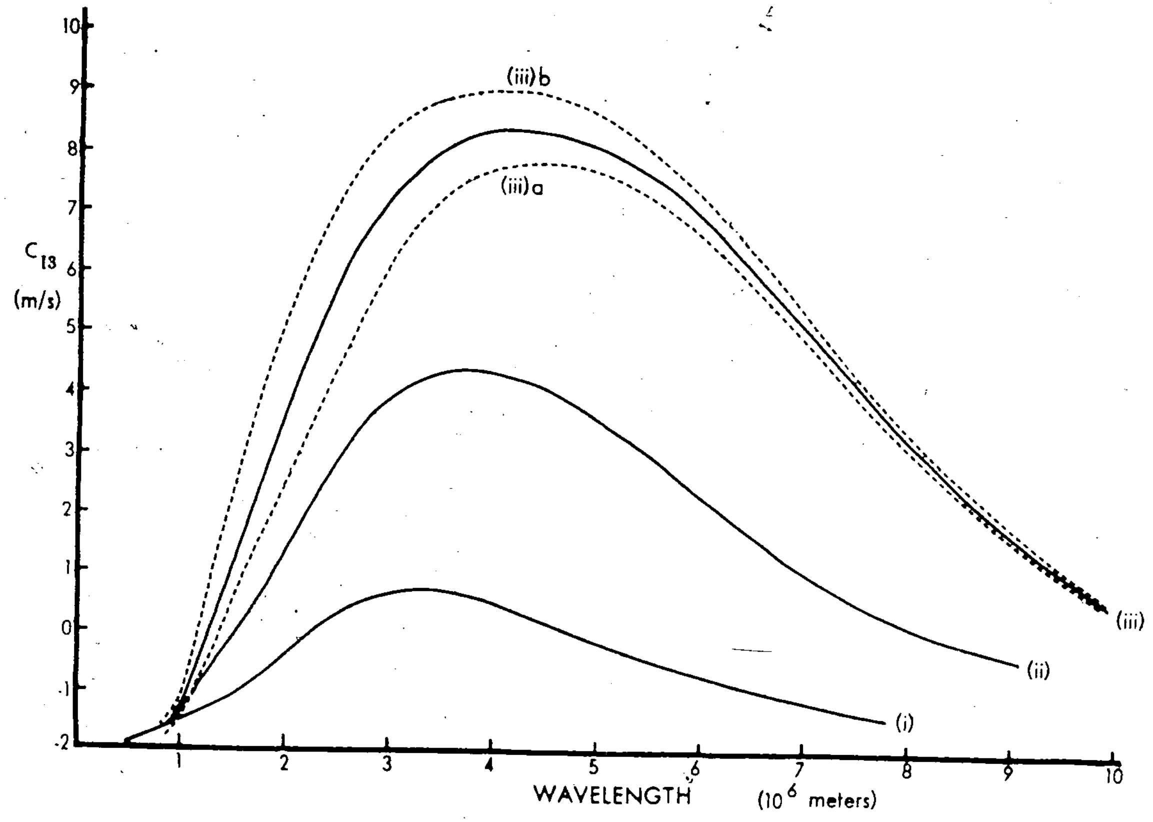

Fig. 4.4. Response of the stability curve c_{I3} to changes in the mean wind shear and mean static stability. The solid curves are for a constant static stability of $\bar{\sigma} = 12^oC$ with vertical wind shear values of (i) 5 m/s, (ii) 10 m/s and (iii) 15 m/s. The dashed curves have a constant vertical shear of $U_T = 15$ m/s for mean static stabilities of (iii)a 15°C and (iii)b 9°C. All calculations were taken from model 4 with all other quantities kept constant.

of the atmosphere was increased the instability of the perturbation field was reduced. This reduction is much more significant at the lower end of the wavelength range and became marginal at larger L_x values. The relative propagation rate of shorter waves was also found to decrease as $\bar{\sigma}$ was increased, but once again this effect diminished at longer wavelengths to the point where the wave speeds were virtually unchanged.

Although the perturbations have been assumed to be latitudinally independent, variations in latitude may still influence the numerical results through the Coriolis parameter and its meridional derivative β. Therefore, the values of these two quantities were varied so as to represent different latitudinal x-axes. At lower latitudes, as suggested by a comparison of the unstable curves in Fig. 4.5, the perturbation field was found to be considerably more stable and the range of unstable wavelengths was reduced significantly. In addition, Fig. 4.5 shows that as latitude decreased the perturbation waves had a greater rate of retrogression with respect to the mean zonal current.

4.4 Perturbation Field as a Function of Latitude

At this time the previous assumption that the perturbation field is independent of latitude is relaxed and the simple cosine variation of (3.3.2) is employed. Unlike wavelengths on the x-axis which have been expressed in

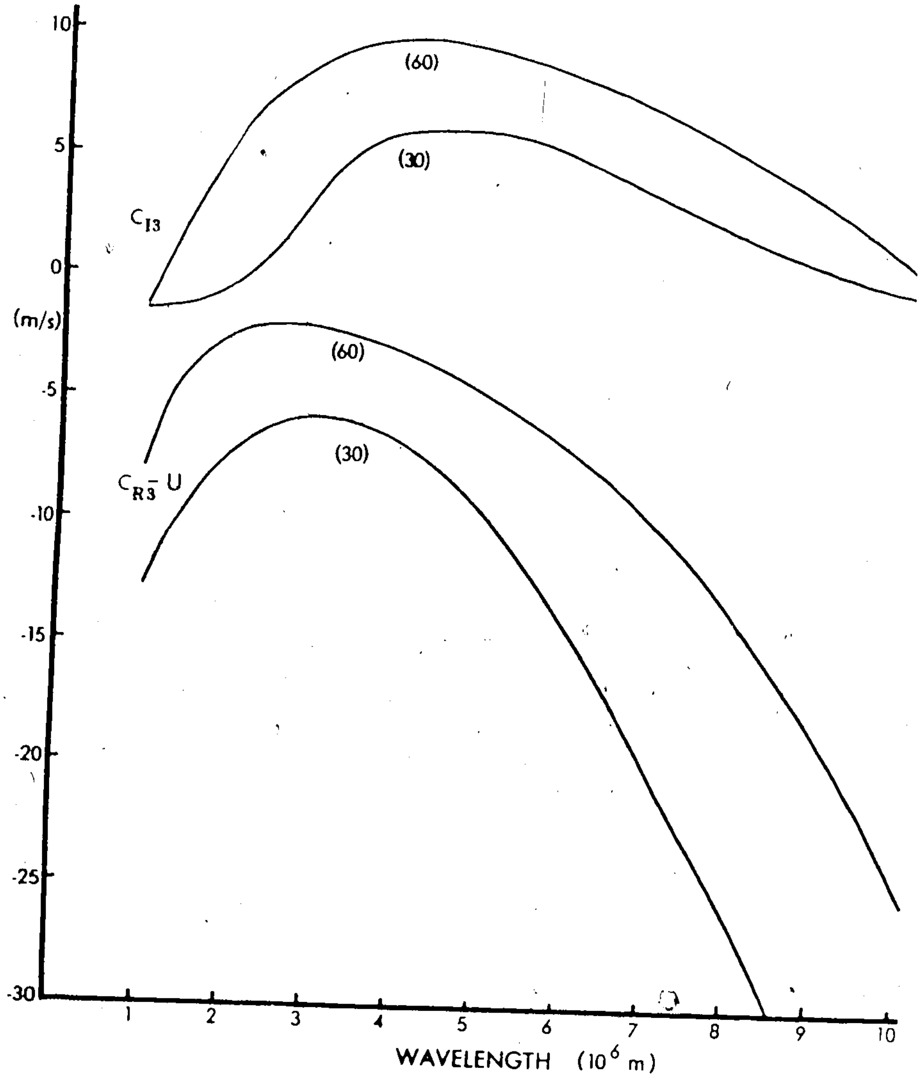

Fig. 4.5. Effect of latitude variations on the stability and propagation rates of unstable waves. The stability curves c_{I3} and relative wavespeed curves $c_{R3} - U$ were computed using model 4 with $U_T = 15$ m/s. Latitude is distinguished by the bracketed values assigned to each curve. In the calculations $f(60N) = 1.263 \times 10^{-4}$ s^{-1}, $\beta(60N) = 1.14 \times 10^{-11}$ m^{-1} s^{-1}, $f(30N) = 7.292 \times 10^{-5}$ s^{-1} and $\beta(30N) = 1.98 \times 10^{-11}$ m^{-1} s^{-1}.

distances of meters or kilometers a meridional wavelength will be given in terms of degrees of latitude. In all cases the origin in the north-south direction will be taken as 45N. The interpretation of L_y=120° is that of a perturbation travelling in an east-west direction having its maximum absolute amplitude at y(45N)=0 and an amplitude which approaches zero at latitudes 75N and 15N.

The computations were redone using the same numerical values as utilized earlier for the steady-state quantities. The full model was run for varying values of $n=2\pi/L_y$. Figure 4.6 shows the phase-velocity response curves $(c_k - U)$ at latitude 45N when L_y=90°. The general shapes of the curves were similar to those shown in Figures 4.1 and 4.2. A comparison of values in Tables 6 and 7 indicates that unstable long waves have greater rates of growth and travel at slower propagation rates after the 90° latitudinal dependence has been introduced into the modelling.

Figure 4.7 illustrates the resulting unstable solution for a range of L_y values between 60° and ∞ ($L_y=\infty$ implies no latitude dependence). The changes that occurred in the c_{I3} values in response to varying values of L_y were similar and, therefore, not all of these curves are shown. In going from $L_y=\infty$ to L_y=60° the amplitude of the c_{I3} curve showed a marginal decrease in amplitude up to a wavelength of L_x=5000 km. At wavelengths L_x>5000 km instability increased and, as a result, the unstable waveband was extended to include longer waves. The relative travelling speeds of the

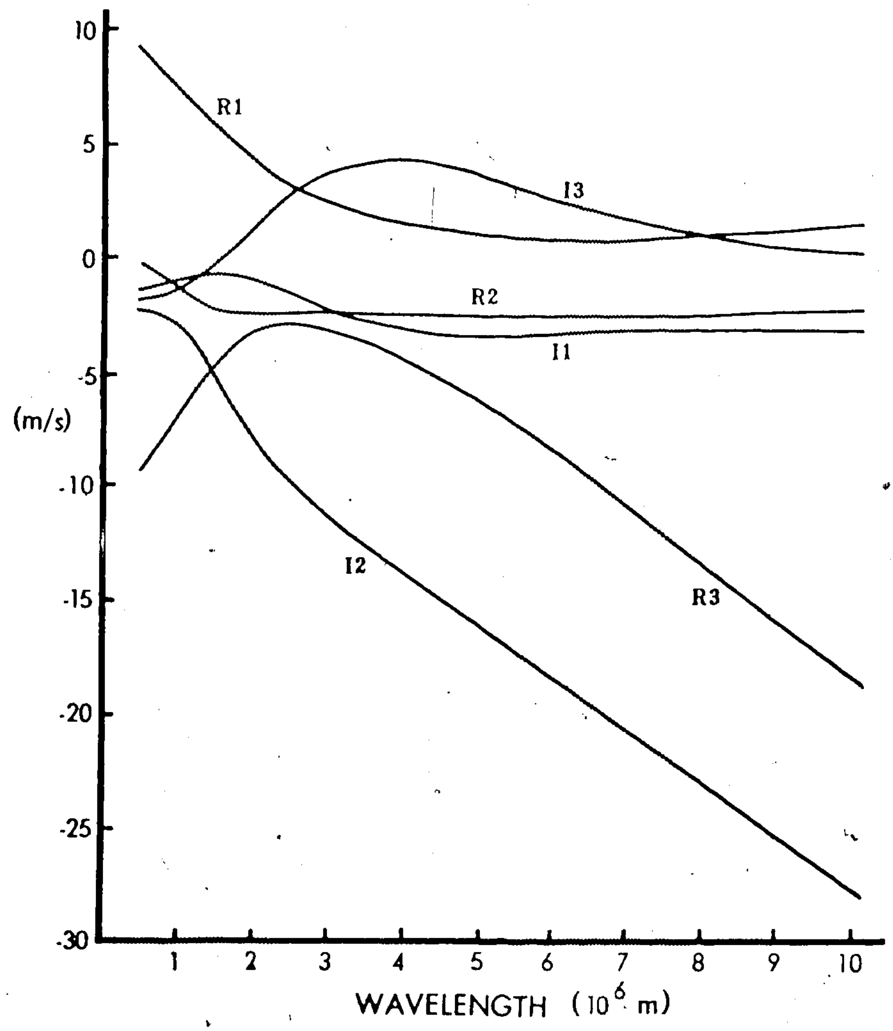

Fig. 4.6. Phase velocity response for the full model incorporating a 90° latitudinal dependence ($L_y = 90°$). Curves R_1, R_2 and R_3 are the real parts and I_1, I_2 and I_3 the corresponding imaginary parts to the frequency equation solutions $(c_k - U)$, $k = 1,2,3$.

Table 7. Real (R3) and imaginary (I3) portions of the phase velocities over the unstable waveband of Fig. 4.6 and the corresponding e-folding times (t_e).

Wavelength (km)	R3 (m/s)	I3 (m/s)	t_e (days)
1500	-4.34	<0	
2000	-3.18	1.54	2.39
2500	-2.80	2.84	1.62
3000	-3.03	3.68	1.50
3500	-3.58	4.10	1.57
4000	-4.31	4.20	1.75
4500	-5.17	4.08	2.03
5000	-6.14	3.81	2.42
5500	-7.22	3.43	2.95
6000	-8.39	2.99	3.70
6500	-9.64	2.54	4.71
7000	-10.94	2.11	6.11
7500	-12.25	1.70	8.13
8000	-13.5[illegible]	1.33	11.08
8500	-14.82	1.00	15.66
9000	-16.05	0.69	24.03
10000	-17.24	0.41	44.93
10500	-18.37	0.15	128.94
11000	-19.44	<0	

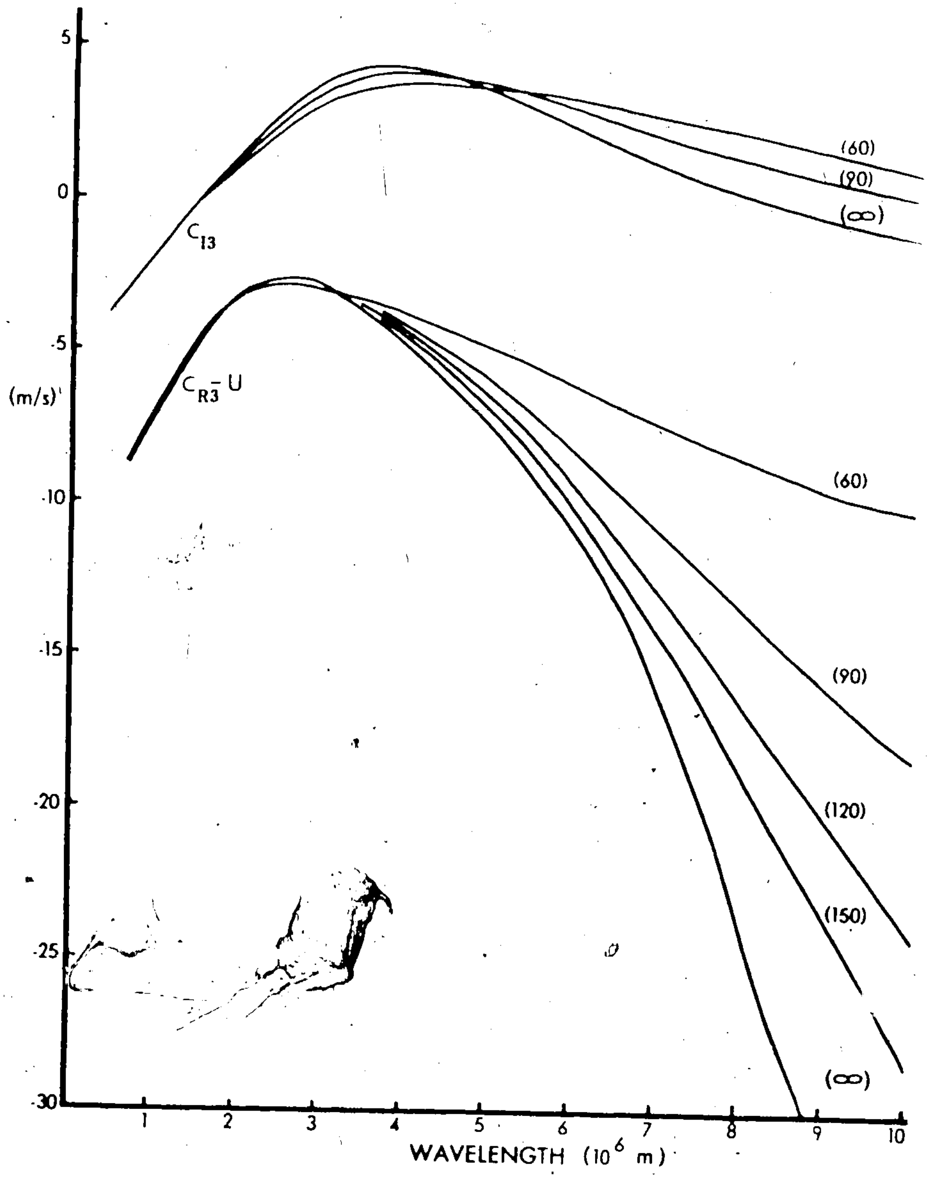

Fig. 4.7. Effect of variations in the meridional wavelength L_y on the stability and propagation of unstable waves. Numerical results for the stability curves c_{I3} were computed using the full model and $L_y = 60^\circ$, 90° and ∞ as indicated by the bracketed values assigned to each curve. For the relative wavespeed curves the scope of L_y values was expanded to include $L_y = 120^\circ$ and 150°. The curves for $L_y = \infty$ are interpreted as having no latitudinal dependence and are, therefore, analogous to curves of model 4.

unstable waves were affected in a similar manner. Up to values of L_x=4000 km the propagation rates of the waves were almost unchanged. At values greater than 4000 km reductions in the magnitude of L_y resulted in the waves experiencing propagation rates which more closely approached the speed of the steady-state current.

If y is taken to be non-zero in the model then the absolute amplitude of the perturbation field is reduced. This in itself has little bearing on the dynamic stability of the flow if the ratio y/L_y is less than 1/4 (i.e. if $y/L_y \simeq 1/4$ then $\tan(ny) \rightarrow \infty$ in the coefficient b^{15}). A value of $y \neq 0$, however, implies higher or lower latitudes and the main changes in the relative phase velocity curves occur because of changes in f and β as was seen previously in Fig. 4.

4.5 Amplitude and Phase Relationships

Phase velocity solutions to the frequency equation determine the stability features of the perturbation field. However, stability curves do not show directly the interactions of the three wave solutions or the relationships between the various perturbation quantities. The initial-value technique outlined in Chapter 3 will now be used to extend the analysis to include such interactions and interelationships. The following parameters were held constant: U=20 m/s, U_T=10 m/s, L_y=90°, $k_t=10^{-2}$ J/(kg s °C), $\bar{\sigma}$=12°C, $k_s=4\times10^{-6}$ s^{-1}, $K_M=K_H=10^5$ m^2/s and $k_c=k_h=10^{-6}$ s^{-1}

with f and β evaluated at a latitude of 45N. In addition, the initial amplitudes assigned to the stream function, potential temperature and static stability perturbation waves were held constant at $\hat{\psi}_0 = 9.806 \times 10^6$ m^2/s, $\hat{\theta}_0 = 10$°C and $\hat{\sigma}_0 = 2$°C. In order to obtain estimates of the magnitude of the stream function it is useful to assume from the linear balance equation that $\hat{\phi}_0 = \hat{\psi}_0 \bar{f}/g$ where the mean Coriolis parameter can be taken as being approximately 10^{-4} s^{-1}. Therefore, the averaged value of the stream function can be thought of in terms of a geopotential height with an initial amplitude of 100 m. In the future $\hat{\psi}_A$ will be expressed in its geopotential 'equivalent' in units of meters.

Figures 4.8 and 4.9 show the characteristic curves for a wavelength of 4000 km taken from model 4. The initial phase angles ε_θ and ε_σ in Fig. 4.8 were both taken to be 90° meaning that the potential temperature and stability waves lagged behind the stream function. These angles were changed to -90° in Fig. 4.9. The 4000 km wavelength is indicative of the middle range of the instability waveband where growth rates are quite large.

The rate of amplification for the different perturbation quantities as displayed in Fig. 4.8a was quite rapid during a 72-hour period. It is also apparent that, except for a time during the first 12 hours when the amplitude of the static stability briefly decreased, the amplification rate of each perturbation increased in time.

Figure 4.8b displays all phase angles in degrees. If a

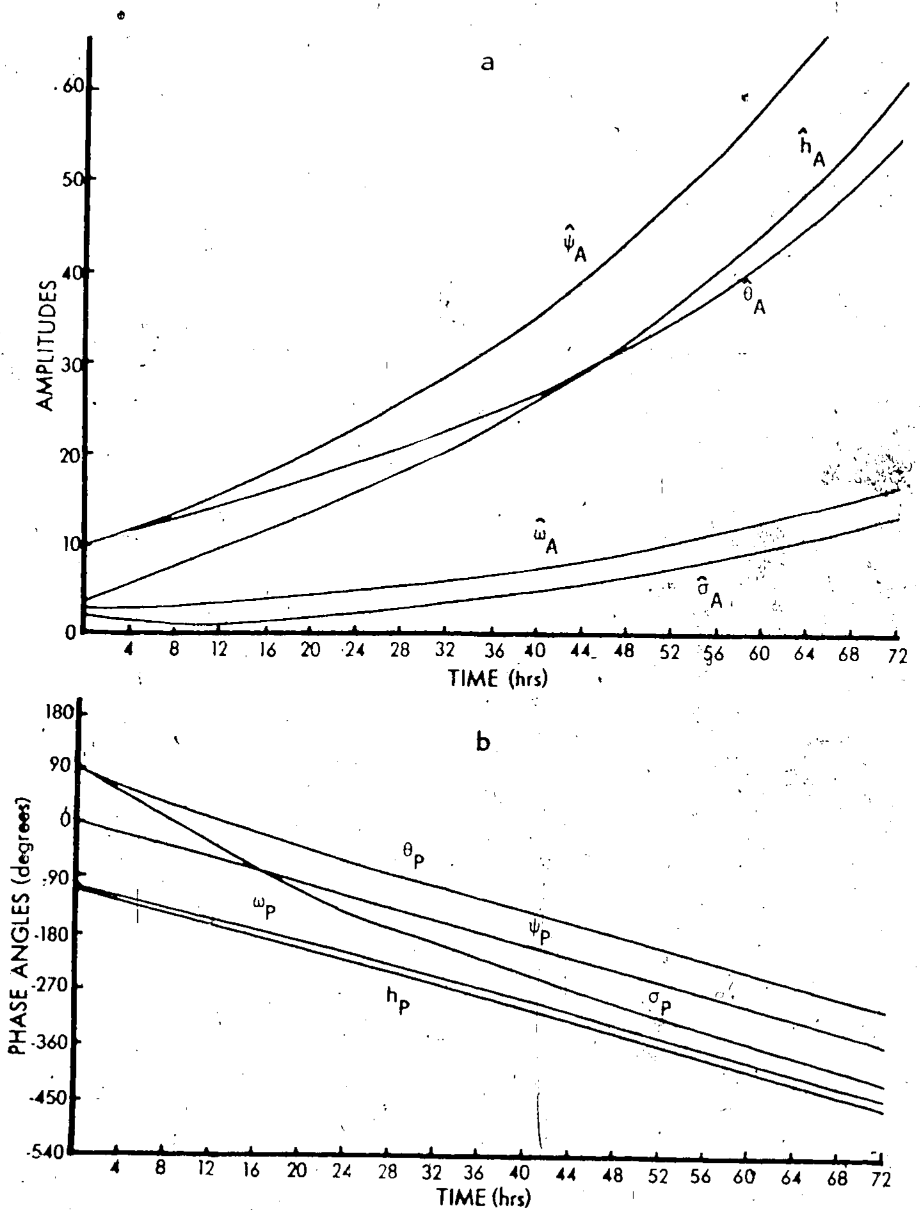

Fig. 4.8. Perturbation amplitudes and phase angles as functions of time for model 4 with L_x = 4000 km, U = 20 m/s, U_T = 10 m/s, $\varepsilon_\theta = 90^\circ$ and $\varepsilon_\sigma = 90^\circ$. Amplitudes in (a) are $\hat{\psi}_A(10^1\text{m})$, $\hat{\theta}_A(^\circ\text{C})$, $\hat{\sigma}_A(^\circ\text{C})$, $\hat{\omega}_A(10^{-4}$ kPa/s) and $\hat{h}_A(10^{-2}$ J/(kg s)). Phase angles in (b) are in degrees.

curve slopes towards lower (negative) phase angle values the wave in question is progressing in an easterly direction. A slope to higher (positive) phase angles thus represents retrogression westwards. All of the perturbation waves depicted in this figure travelled eastwards and the short interval when $\hat{\sigma}_A$ is damped is seen to correspond to a time when the static stability wave advanced toward the stream function.

The growth curves for Fig. 4.9a are slightly changed from those of the previous case. The stream function was damped initially for 24 hours while the potential temperature wave advanced to within a lag of approximately 130° (Fig. 4.9b), after which the stream fuction began to amplify. In addition, the former wave's eastward motion was reduced substantially between 12 and 24 hours until the potential temperature wave had moved into this appropriate lag position. The potential temperature wave can be interpreted as a 'thermal' wave since it uniquely determines the value of η' which is representative of a geopotential thickness in the same manner that ψ' is representative of height. Thus, the thermal wave necessarily lags the geopotental height wave in order for amplification of the height field to occur. Static stability increased during this initial time period and then subsequently showed a short period of damping. A large drop in the surface heating amplitude was noticed during the first few hours as this wave moved rapidly from a trailing position behind the

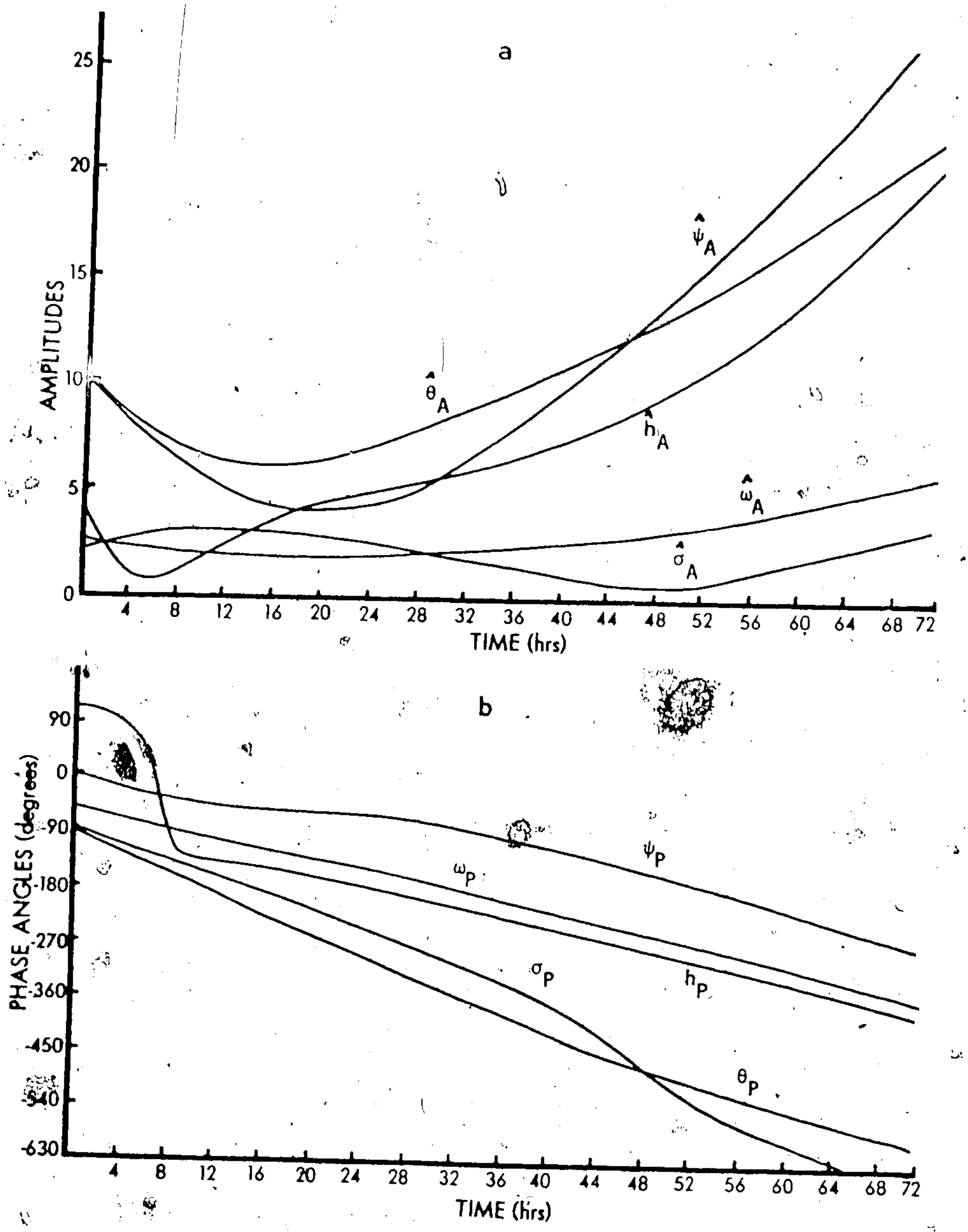

[illegible] 4.9. Perturbation amplitudes and phase angles as functions of time for model 4 with L_x = 4000 km, U = 20 m/s, U_T = 10 m/s, $\varepsilon_\theta = 90^\circ$ and $\varepsilon_\sigma = -90^\circ$. Amplitudes in (a) are $\hat{\psi}_A(10^1\,m)$, $\hat{\theta}_A(^\circ C)$, $\hat{\sigma}_A(^\circ C)$, $\hat{\omega}_A(10^{-4}$ kPa/s) and $\hat{h}_A(10^{-2}$ J/(kg s)). Phase angles in (b) are in degrees.

stream fuction wave into a phase lead.

Many runs were made with L_x=4000 km for different values of ε_θ, ε_σ and with various model types. The adiabatic-frictionless results of model 1 corresponding to the two cases already discussed have qualitatively the same growth and phase relations as when friction and sensible heating are included. In general, however, model 1 gave the greatest amplification of the waves during the 72-hour period.

Certain phase difference values showed characteristic changes depending on whether heating or frictional effects were included in the modelling. As an example, in Fig. 4.8b the difference $\theta_p - \psi_p$ at the end of 72 hours was 56°. In model 2, using the same initial conditions, this phase difference was 63° while model 1 gave a final value of 73°. Thus, friction and sensible heating had the effect of allowing the thermal wave to approach a position somewhat closer behind the geopotential height wave during amplification. Other runs using different initial phase conditions values also supported these trends between the various model types.

More pronounced changes were seen in the values of $\sigma_p - \psi_p$. In Fig. 4.8b the static stability overtook the stream function in 12 hours after which it slowly moved to a 56° lead by t=72 hr. Adding a 90° latitudinal dependence in the full model did not alter this value and dropping friction from the modelling resulted in only a 5° decrease in the phase difference. Model 1, however, had a final phase lead value of 114°, a rather significant change which can be attributed to the lack of sensible heating. Once more this trend was supported in other runs with various initial conditions.

The surface heating and vertical velocity perturbation fields showed evidence of having consistent phase relations with the stream function. Surface sensible heating was found to lead the stream function during maximum growth of the waves by a phase angle of 108-114°. This would put the maximum heat input from the earth's sur[illegible] to the atmosphere in a position upstream of the trough position and the zone of maximum cooling upstream of the ridge during amplification.

In those instances when friction was not included in the modelling the vertical velocity wave led the stream function by approximately 102° indicating that maximum downward velocities in the mid-troposphere occurred between the ridge and the downstream trough position. When friction was added this phase lead was reduced by 4 or 5 degrees.

Figures 4.10 and 4.11 show the curves for a wavelength of L_x=7000 km. Such a wavelength is representative of long waves where the degree of instability is decidedly less than that of intermediate wavelengths near 4000 km. In both cases shown the initial phase angles were 90°. Figure 4.10 illustrates model 4 while Fig. 4.11 pertains to the full model.

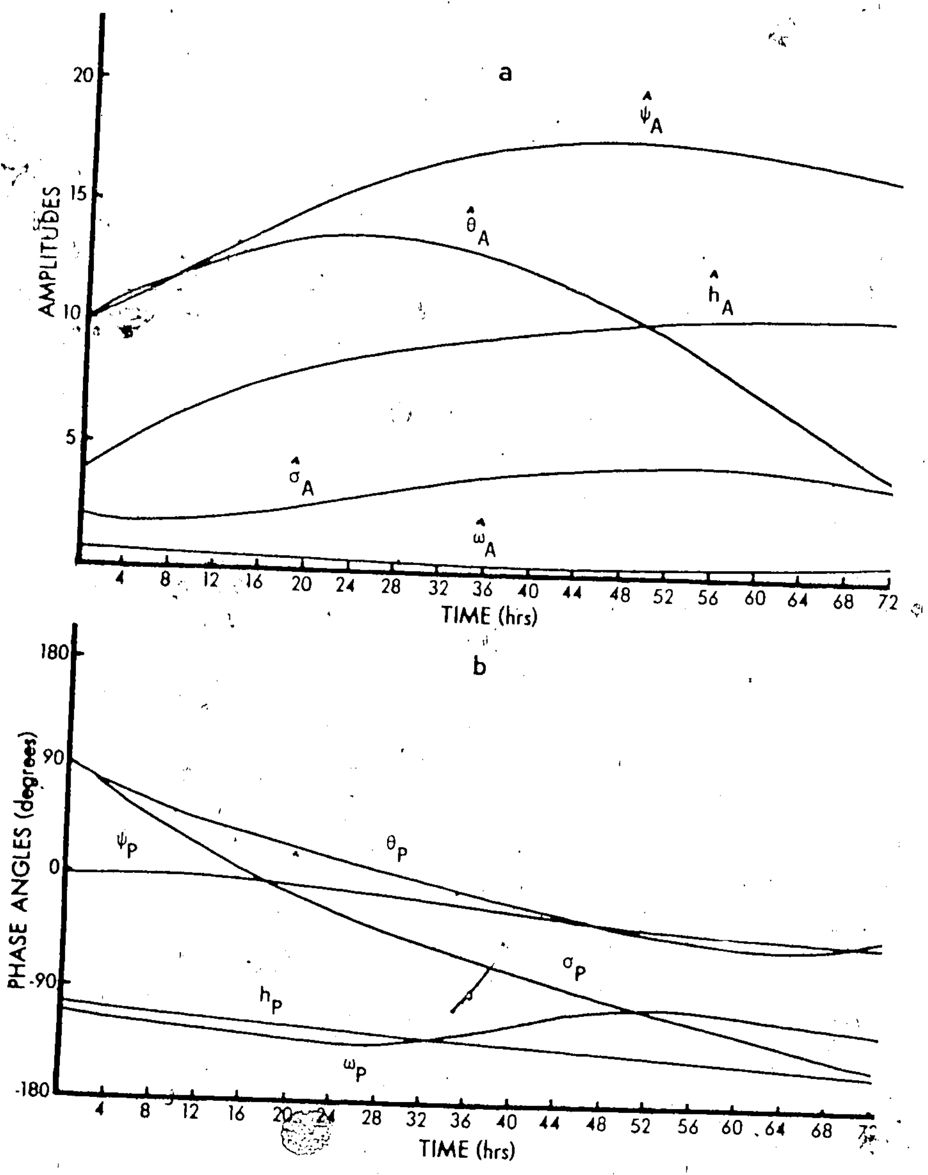

Fig. 4.10. Perturbation amplitudes and phase angles as functions of time for model 4 with L_x = 7000 km, U = 20 m/s, U_T = 10 m/s, $\varepsilon_\theta = 90^\circ$ and $\varepsilon_\sigma = 90^\circ$. Amplitudes in (a) are $\hat\psi_A(10^1 m)$, $\hat\theta_A(^\circ C)$, $\hat\sigma_A(^\circ C)$, $\hat\omega_A(10^{-4}$ kPa/s) and $\hat h_A(10^{-2}$ J/kg s)). Phase angles in (b) are in degrees.

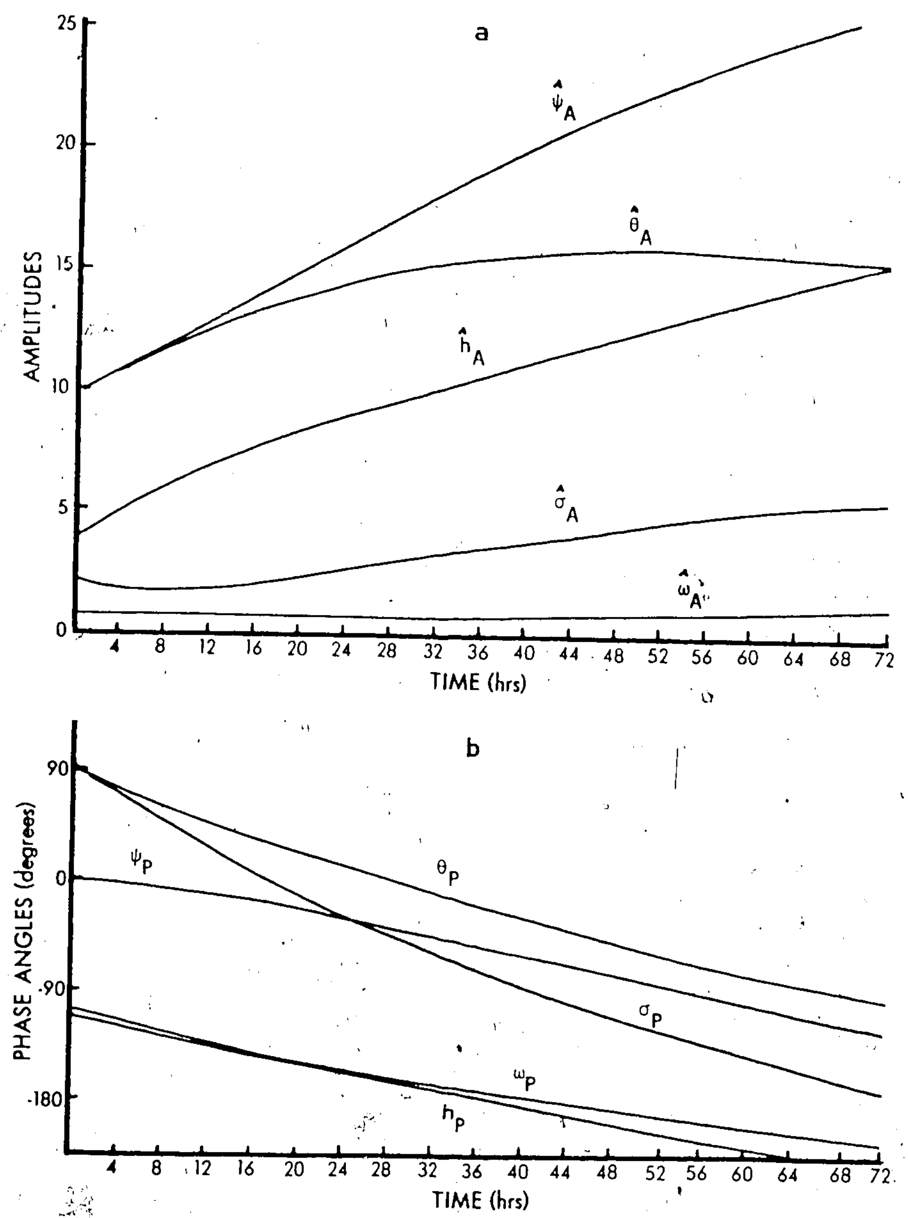

Fig. 4.11. Perturbation amplitudes and phase angles as functions of time for the full model with $L_y = 90^{\circ}$, $L_x = 7000$ km, $U = 20$ m/s, $U_T = 10$ m/s, $\varepsilon_\theta = 90^{\circ}$ and $\varepsilon_\sigma = 90^{\circ}$. Amplitudes in (a) are $\hat{\psi}_A(10^{1}\,m)$, $\hat{\theta}_A(^{\circ}C)$, $\hat{\sigma}_A(^{\circ}C)$, $\hat{\omega}_A(10^{-4}$ kPa/s) and $\hat{h}_A(10^{-2}$ J/(kg s)). Phase angles in (b) are in degrees.

Several noteworthy differences are seen in these curves when they are compared with the previous results for L_x=4000 km. As expected the perturbations now underwent a far lesser rate of growth than seen previously and they moved at slower speeds as depicted by the shallower slope to the phase angle curves. As well, the rate of amplification of the waves now generally decreased with time and, in some instances, as illustrated in Fig. 4.10b, the waves experienced retrogressive tendencies.

The first perturbation quantity to show a decrease in amplitude in Fig. 4.10a was the potential temperature. This occurred, according to the phase relations of Fig. 4.10b, when the potential temperature wave moved to within 20-25° of the stream function wave position. Then, as the potential temperature proceeded to overtake the stream function, the value of $\hat{\psi}_A$ also showed a reduction in amplitude. This is consistent with the concept of the thermal wave overtaking the height wave and thereby terminating amplification. In the latter part of the 72-hour period the potential temperature wave continued steadily moving away from the stream function which in turn began to retrogress slowly.

Previously the perturbation field with L_x=7000 km was observed to have greater instability and faster propagation rates once a meridional variation was inserted into the modelling. These features are now reflected in Figs. 4.11a and 4.11b where by t=72 hours the perturbation quantities had all undergone greater amplification and had progressed further east than in the preceding case. The increased amplification is the result of the fact that the potential temperature never quite overtook the stream function wave and maintained a minimum lag of 22°.

Changing the initial phase angles when $L_x = 7000$ km invoked much the same behavior in the phase angle and amplitude curves as was observed with the shorter wavelength of 4000 km. Greater amplification was found to occur when ε_θ was taken to be positive (lag) and ε_σ negative (lead) rather than reversing this arrangement. Of those numerical computations performed where sensible heating was included, the longer 7000 km waves showed the greatest amplification rates when ε_θ was 180°. This arrangement implies that the thermal wave is initially exactly out of phase with the stream function wave and thus a warm trough and cold ridge structure is present.

In most cases 72 hours was not enough time to establish any definite phase relationship between the static stability and stream function for the longer 7000 km wave. During times of steady increases in $\hat{\psi}_A$ the vertical velocity wave was found typically to precede the stream function wave by 125° to 155°. This lead was shortened to as little as 60° when the stream function experienced weaker rates of growth or underwent slight damping. It should also be noted that the magnitude of the vertical velocity field was almost an order of magnitude less than that found at the shorter wavelength L_x =4000 km. The surface heating wave tended to remained downstream of the ridge position in the calculations with a leading phase angle of 120° to 130° with respect to the stream function wave.

At wavelengths longer than 7000 km the perturbation field continued its trend to slower growth and greater retrogressive motion. The 72-hour period of calculations was insufficient to determine many consistent phase relationships between the quantities although the behavior of the waves is somewhat similar to the L_x=7000 km results.

4.6 Blocking Ridge Development Over the North Pacific

Blocking ridge activity, as interpreted by Rex (1950a), exhibits several distinguishing characteristics in its mid-tropospheric flow. These characteristics were defined as:

(i) a sharp transition from more or less zonal westerlies upstream to a meridional type of flow downstream must occur with a block;

(ii) the basic westerly flow should have split into two branch streams with each branch transporting appreciable mass; and

(iii) the two-jet pattern must exist with an extension of 45° of longitude or more downstream from the split and must persist for a minimal ten days.

As an example of such ridging occurrences a detailed case study of an Atlantic block was presented in the Rex (1950a) investigation. This particular ridging lasted for more than 20 days of which the first week could be described as being the growth time required to develop a recognizable block from a basic onal flow.

In subsequent investigations Rex (1950b, 1951) found that blocking showed a seasonal and spatial preference for its formation; preferring the winter months over that of the summer and an ocean environment over that of a continental location. He also determined that blocking normally persisted for 2 to 3 weeks after its formation with very little overall motion during its entire lifetime.

Whereas Rex employed daily synoptic charts in his studies, White and Clark (1975) used monthly mean data to investigate the occurrence of blocking activity over the North Pacific. This precluded the authors' ability to determine specific growth or duration times for blocking and it could only be established that the blocking had occurred long enough to have affected the mean monthly pressure pattern in the mid-troposphere. In defining what was considered as an oceanic block this study excluded all ridging waves which formed and were centered over the western part of North America as being a form of amplified mountain waves.

Some of White and Clark's results have been mentioned in Chapter 1. As shown in Fig. 4.12 the data revealed a preference for winter blocks which had a characteristic wavelength of 6000 to 7000 km centered over a longitudinal position of 160W to 170W. The blocking activity was also found rarely to exceed two months in length at any given period of the year and was apatially correlated with

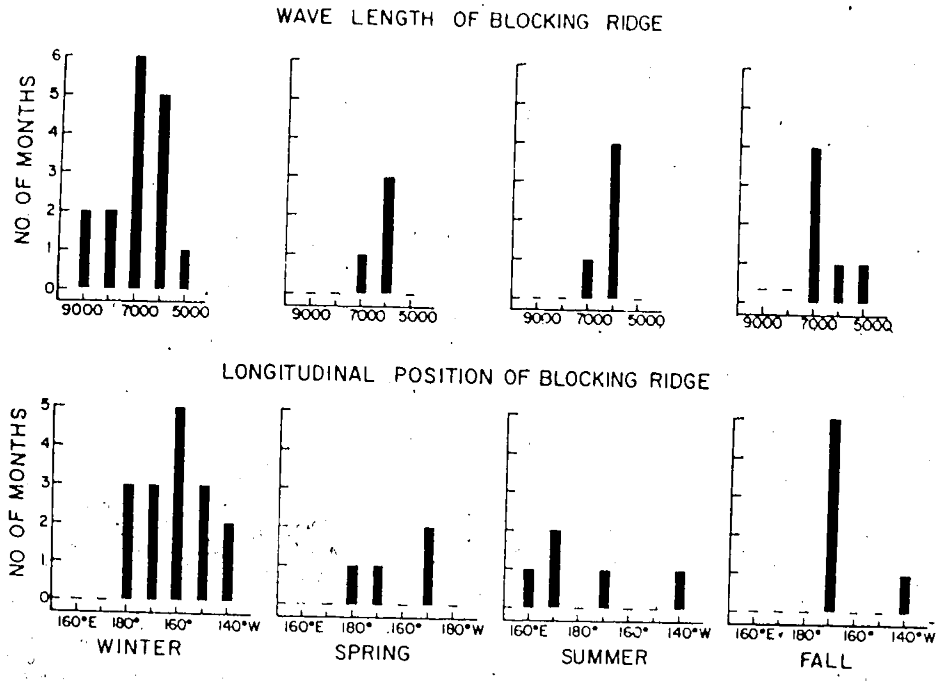

Fig. 4.12. Seasonal and spatial variability of North Pacific blocking ridges as given by White and Clark (1975). The histograms were based on monthly mean data over a period from 1950 to 1970. The seasons were defined as being; winter (January-March), spring (April-June), summer (July-September) and autumn (October-December).

patterns of anomalous surface sensible heat flux (cooling under the ridge position). It was the authors' conclusion that Haltiner's (1967) predictions of slow moving or stationary unstable longwave growth explained some of these observations and, therefore, supplied theoretical support for their findings. However, upon closer look at the argument presented there would seem to have been some misinterpretation of Haltiner's results on their part.

During their discussion White and Clark presented Fig

4.13 as Haltiner's unstable phase velocity solutions for

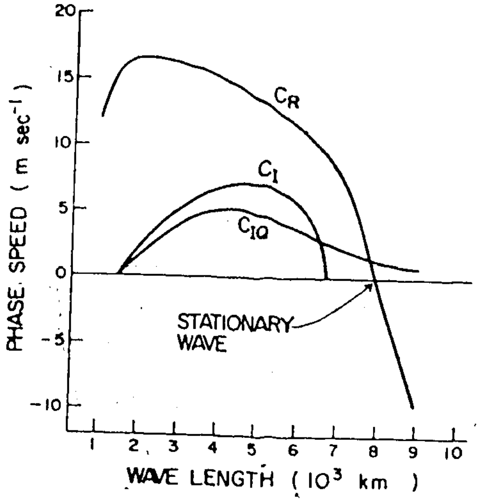

Fig. 4.13. The real (C_R) and com[illegible] (C_I) parts of the phase speed for baroclinic unstable waves as [illegible] in White and Clark (1975). The diabatic and adiabatic stabil[illegible]ves are denoted by C_{IQ} and C_I, respectively. Values are based on Haltiner's (1967) numerical results. The mean vertical wind shear and mean zonal wind were given as U_T = 10 m/s and U = 30 m/s in White and Clark's discussion, however, Haltiner's theory utilized a mean zonal wind of only 20 m/s in obtaining these curves.

U=30 m/s, U_T=10 m/s and conditions with sensible heat transfer and without. In reality these curves are obta[illegible] for a mean zonal wind of only 20 m/s. It is also left to interpretation in the White and Clark study that the real portion of the phase velocity (C_R) of Fig. 4.13 applies to both the adiabatic and diabatic cases. This is misleading since the C_R curve shown is valid only for the adiabatic case. The diabatic version of this curve for U=20 m/s gives a stationary wave of approximately 7600 km which is some 300 to 400 km shorter than the 8000 km found for the adiabatic curve. If U is taken to be 30 m/s as is used throughout the White and Clark discussion, the diabatic model as indicated in Table 4 gives a stationary unstable wave of L_x=9000 km. This would then be well beyond the 8000 km value shown in Fig. 4.13.

The behavior of Haltiner's amplified waves has been likened to that of Rossby-type waves. The Rossby dispersion relation of;

$$L_s = 2\pi \left(\frac{U}{\beta}\right)^{1/2} \qquad (4.6.1)$$

might therefore be used to predict the wavelength, L_s, of a stationary Rossby-type wave. Applying (4.6.1) with U=30 m/s and β(45N)=1.61X10^{-11} m^{-1}s^{-1} gives a predicted L_s value of 8577 km. If U=20 m/s is substituted into the relation the stationary wavelength diminishes to 7003 km. Neither of these values agrees with a value of 7600 km claimed by White and Clark using (4.6.1) and U=30 m/s. The apparent confusion surrounding White and Clark's argument makes it necessary to reconsider the theoretical predictions and their applicability to the characteristics of North Pacific blocking development.

In order to obtain values for the mean winter zonal wind and vertical wind shear to be employed in the

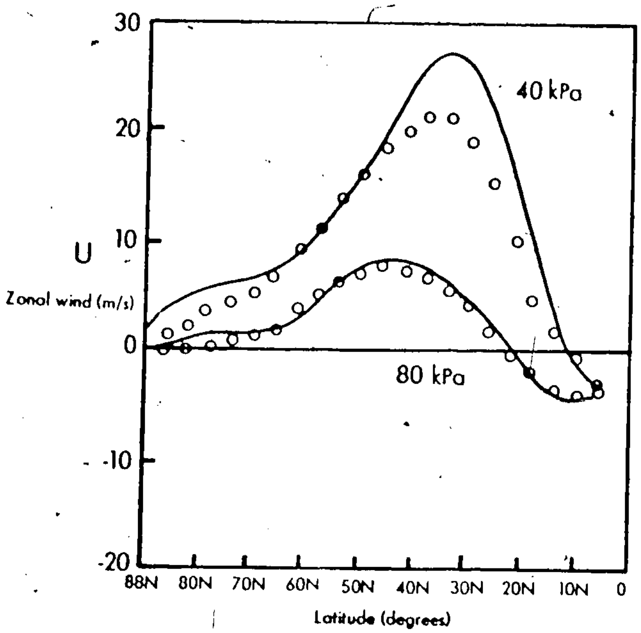

Fig. 4.14. The zonal average of the mean westerly winds for January at 80 and 40 kPa over the Northern Hemisphere as given by Gates (1975). The open circles are zonal averages of the observed mean wind (for December, January, February) based on the data of Crutcher (1961). The solid curves represent the corresponding zonal averages of the observed geostrophic winds as based on the data of Crutcher and Meserve (1970).

computations, use was made of the curves of Fig. 4.14 which are taken from Gates (1975). These curves are based an available observed wind data in the Northern Hemisphere and those mean geostrophic zonal winds which may be calculated from observed geopotential fields. As shown, the zonal average of the 80 kPa westerly wind had a definite maximum value of 8 m/s at approximately 40N to 45N. The observed westerly wind at 40 kPa reached its maximum of just over 21 m/s at 30N to 35N although the geostrophic wind was somewhat stronger at 28 m/s. In terms of vertical wind shear across the two isobaric levels, the greatest difference in the observed mean westerlies was found to occur near 35N and was about 16 m/s. For the geostrophic zonal wind the maximum difference was slightly higher being 20 m/s at about the same latitude.

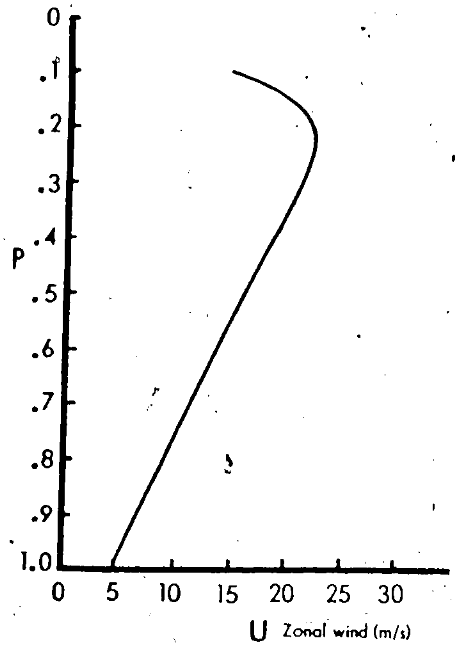

Fig. 4.15. Vertical profile of the observed mean zonal wind for the period December to February at 45N as given by Döös (1962). Values are based on the data of Crutcher (1959). Pressure (ordinate) is given as a non-dimensional variable P = p/p_s where p_s = 90 kPa.

Figure 4.15 taken from Döös (1962) is also based on averaged wind data. It shows the observed zonal wind profile for the winter period December to February at a latitude of 45N. The profile displays an almost constant wind shear through the mid-layers of the troposphere which translates to roughly 12 m/s over the 36 kPa interval between P=0.8 (72 kPa) and P=0.4 (36 kPa).

Based on Figs. 4.14 and 4.15 a representative mean 60 kPa winter value of U at 45N would be approximately 13 or 14 m/s. Since observed year-to-year changes in the autumn/winter mean wind in the lower troposphere are typically in the order of 25% (White and Clark, 1975) and assumed range of values for U was taken to be 14 ± (.25) X (14) m/s, giving a variation from 10.5 to 17.5 m/s. The corresponding mean vertical wind shear in the mid-troposphere was taken as being about 7 m/s over a 20 kPa layer. Normally the mean wind shear in the atmosphere at mid-latitudes does not experience large fluctuations. White and Clark have established that the year-to-year variability in the winter value of the vertical shear for the geostrophic wind between 100 and 70 kPa over the North Pacific is only 5%. Since it is not inconceivable that this also applies to the mid-troposphere a range of values was not assigned to U_T.

It is worth noting that by using U_T=7 m/s the implied mean westerly wind at 50 kPa is close to 17 m/s. If a 25% variation is again instituted the upper estimate becomes 21 m/s which falls significantly short of White and Clark's estimate for the mean winter westerlies of 30 m/s at this level. General circulation studies for January, such as those of Gates (1975) and others, typically show a simulated local mean westerly wind maximum off the east coast of Asia at mid-latitudes which may extend well into the North Pacific. If correct, this implies that the winter value of U may be slightly higher in this region than that derived from the zonally averaged wind data. It is not likely, however, that the increase in the mean wind over the entire North Pacific is enough to account for the rather large difference between the averaged values and that of 30 m/s. It would appear from previous studies by other authors that the lower value of near 20 m/s is more commonly used when an estimate for the mid-latitude 50 kPa mean wind is required.

Earlier it was seen that the modelling is not critically responsive at longer wavelengths to changes in the mean static stability. Therefore, $\bar{\sigma}$ was held constant at 12°C in the computations. Discussion presented in White and Clark's study indicated that the surface sensible heat exchange does not vary significantly during the winter months. Hence, k_t was also given a constant value of 10^{-2} J/(kg s °C) during the calculations.

The adiabatic version (model 1) did not predict the possibility of stationary unstable wave growth when U_T=7 m/s and U=10.5 to 17.5 m/s were used in the calculations. This was not the case when sensible heating was incorporated. Table 8 summarizes the phase velocity solutions of model 2 for those wavelengths with which the possibility of a stationary unstable existed. From this table it is

Table 8. Unstable wavelengths (L_x) and the corresponding e-folding times (t_e) for model 2 (diabatic, frictionless flow) using $U_T = 7$ m/s and $k_t = 10^{-2}$ J/(kg s °C) over a relative phase velocity range of approximately -10.5 to -17.5 m/s.

L_x (km)	t_e (days)	$c_{R3} - U$ (m/s)
5500	6.5	-10.1
5600	6.9	-10.6
5700	7.3	-11.1
5800	7.8	-11.6
5900	8.2	-12.1
6000	8.8	-12.7
6100	9.3	-13.2
6200	9.7	-13.7
6300	10.4	-14.3
6400	10.9	-14.8
6500	11.5	-15.4
6600	12.0	-16.0
6700	12.7	-16.6
6800	13.3	-17.1
6900	14.0	-17.7

conceivable that a wave within a wavelength band of 5500 to 6800 km could undergo stationary amplification. The upper end of this waveband would require a slightly above average westerly wind and longer growth times while the shorter wavelengths would give fairly rapid development with a weaker zonal flow. In general the waveband was centered about a value of L_x=6200 km which had a relative wave speed of about 14 m/s and an e-folding time of approximately 10 days. These values are in good agreement with characteristic growth times of blocking (1 to 2 weeks), the previous estimate of the mean westerlies and observations of winter blocking ridge activity over the North Pacific. Model 2, however, includes only sensible heating effects. The question therefore arises as to whether incorporation of friction in the modelling might also give similar predictions.

Table 9 reviews the results of model 3 for U_T=7 m/s. The addition of friction to the adiabatic flow produced only a very narrow band of possibilities for stationary wave growth, ranging from 6000 to 6300 km. A look at the e-folding times shows that, except for L_x=6000 km, the growth rates of these waves were very slow. It is, therefore, unlikely that friction alone could result in stationary wave amplification within the model of the same time and space scales as atmospheric blocking.

Calculations were then done for model 4 which incorporates sensible heat exchange and friction

Table 9. Unstable wavelengths (L_x) and the corresponding e-folding times (t_e) for model 3 (adiabatic flow with friction) using $U_T = 7$ m/s and $k_s = 4 \times 10^{-6}$ s^{-1} over a relative phase velocity range of approximately -10.5 to -17.5 m/s.

L_x (km)	t_e (days)	$c_{R3} - U$ (m/s)
5900	10.0	-10.1
6000	14.2	-10.7
6100	22.5	-11.3
6200	42.3	-11.9
6300	166	-12.6
6400	-	-13.2

simultaneously. The waveband of interest was determined as being from 5500 to 6200 km (Table 10). In almost all cases within this waveband the mean westerly wind was necessarily slightly less than its long term mean of 14 m/s for stationary wave development. The growth rates of these waves, as indicated in Table 10, were a little too slow to describe blocking development and the central value of the range of wavelengths was a rather short 5800 km. Such a wave would require a mean westerly wind of only 12 m/s to become quasistationary, but almost a month to increase its amplitude by a factor of e. The addition of frictional

Table 10. Unstable wavelengths (L_x) and the corresponding e-folding times (t_e) for model 4 using U_T = 7 m/s. Surface heating and friction constants used were $k_t = 10^{-2}$ J/(kg m °C) and $k_s = 4 \times 10^{-6}$ s^{-1}, respectively. The relative phase velocity range is approximately -10.5 to -17.5 m/s.

L_x (km)	t_e (days)	$c_{R3} - U$ (m/s)
5400	14.4	-10.3
5500	16.6	-10.8
5600	19.8	-11.3
5700	23.9	-11.8
5800	29.7	-12.2
5900	38.8	-12.7
6000	55.3	-13.3
6100	86.4	-13.8
6200	228	-14.3
6300	-	-14.8

effects to the model has to a certain extent offset some of the congruity between the predictions of model 2 and observed characteristics of North Pacific blocking.

It should be cautioned that the value chosen for U_T in these calculations was critical. For instance, Table 11 is taken from model 4 under the same conditions as before except that now U_T=8 m/s. The range of possible stationary

Table 11. Unstable wavelengths (L_x) and the corresponding e-folding times (t_e) for model 4 using $k_t = 10^{-2}$ J/(kg m/s) and $k_s = 4 \times 10^{-6}$ s^{-1}. Vertical wind shear has been increased to $U_T = 8$ m/s in the calculations. The relative phase velocity range remains unchanged at roughly -10.5 to -17.5 m/s.

L_x (km)	t_e (days)	$c_{R3} - U$ (m/s)
5500	6.2	-10.4
5600	8.7	-10.9
5700	9.7	-11.3
5800	10.8	-11.8
5900	12.2	-12.3
6000	14.0	-12.8
6100	16.1	-13.3
6200	18.7	-13.9
6300	22.3	-14.4
6400	27.4	-14.9
6500	34.2	-15.5
6600	45.7	-16.0
6700	68.6	-16.6
6800	114	-17.2
6900	424	-17.8

unstable waves was found to exist from 5600 to 6800 km. The central value of near 6200 km had an e-folding time of roughly 19 days and required a mean zonal wind of 14 m/s to maintain a quasistationary position. The e-folding growth time is slightly greater than found for atmospheric blocking, but otherwise the values are in agreement once more with observations of winter blocking over the North Pacific and the estimate of the mean westerly wind speed. Therefore, if friction is included in the modelling in addition to sensible heating, a 1 m/s increase in the value of U_T was required to overcome its influence. This might suggest that atmospheric blocking occurs in the presence of friction if the mean vertical wind shear in the mid-troposphere is slightly above its long term mean value. Without the presence of sensible heating, however, stationary wave growth as predicted by the modelling is not likely to occur. This may explain the observed decrease in atmospheric blocking activity over the North Pacific during the summer months since at this time sensible heat exchange between the ocean and atmosphere is greatly reduced.

In studies where the mid-latitude standing wave problem has been investigated by means of linear steady-state models, it has been found that certain meridional wavelengths for the harmonic perturbations give more reasonable results than others when substituted into the equations. Such was the case in the present study for computations based on the full model version of the equations. Table 12 summarizes the results for three different meridional wavelengths: L_y=60°, 90° and 120°. The value of U_T was again taken to be 7 m/s. With L_y=60° the full model does not predict the possibility of a stationary unstable wave within the 10.5 to 17.5 m/s range selected for the winter value of U. When the meridional wavelength is changed to 90° a small band of unstable stationary waves was possible between L_x=6400 and 7000 km. However, the growth rates for the waves within this waveband were very slow, being of the order of one to several months. The last value, L_y=120°, yielded possible stationary wave amplification between approximately 5900 and 6700 km. Once again the e-folding times were fairly large, although at the shorter end of the waveband t_e had decreased to about 3 weeks.

In general the full model, when used with U_T=7 m/s and L_y=60° or 90°, did not satisfactorily describe winter blocking activity over the North Pacific. With L_y=120° the full model predictions were similar to those of model 4 except in one significant regard, this being the value of the central wavelength within the waveband of possible stationary unstable amplification. In the last column of Table 12 this central wavelength is in the vicinity of 6300 km which is some 400 to 500 km longer than the central wavelength predicted by model 4 (Table 10), yet the e-folding times are comparable. The longer 6300 km value lies in the middle of the observed mean wavelength range of

Table 12. Unstable wave solutions for the full model using $U_T = 7$ m/s, $k_t = 10^{-2}$ J/(kg s ^{o}C) and $k_s = 4 \times 10^{-6}$ s^{-1}. The y-axis wavelengths (L_y) are given in degrees of latitude with the origin y = 0 at 45N. The x-axis wavelength (L_x) interval of interest is between 5500 and 7500 km. Relative phase velocities (c_{R3} - U) are given in units of m/s with e-folding times (t_e) expressed in units of days.

	$L_y = 60^o$		$L_y = 90^o$		$L_y = 120^o$	
L_x (km)	t_e	c_{R3} - U	t_e	c_{R3} - U	t_e	c_{R3} - U
5500	8.4	-6.1	10.3	-8.0	12.1	-9.0
5600	9.0	-6.2	11.3	-8.3	13.4	-9.4
5700	9.6	-6.4	12.5	-8.6	15.2	-9.7
5800	10.3	-6.5	13.9	-8.8	17.2	-10.1
5900	11.0	-6.7	15.3	-9.1	19.8	-10.4
6000	11.9	-6.8	17.3	-9.4	23.0	-10.8
6100	12.8	-6.9	19.4	-9.6	27.4	-11.1
6200	13.8	-7.1	22.0	-9.9	33.6	-11.5
6300	14.9	-7.3	25.2	-10.2	41.4	-11.8
6400	16.1	-7.5	29.5	-10.5	56.1	-12.2
6500	17.6	-7.7	35.2	-10.7	79.8	-12.6
6600	19.6	-7.8	43.4	-11.0	135	-12.9
6700	21.7	-7.9	56.0	-11.3	411	-13.3
6800	23.6	-8.1	78.3	-11.6	-	-13.6
6900	26.5	-8.2	114	-11.8		
7000	30.0	-8.4	258	-12.1		
7100	34.4	-8.5	-	-12.4		
7200	40.2	-8.6				
7300	46.4	-8.7				
7400	56.8	-8.9				
7500	72.7	-9.0				

Table 13. Unstable wave solutions for the full model with the mean vertical wind shear, $U_T = 8$ m/s. The respective surface constants for sensible heating and friction are $k_t = 10^{-2}$ J/(kg s °C) and $k_s = 4 \times 10^{-6}$ s^{-1}. The y-axis dependence is taken as being 120 degrees of latitude. Values shown are for a relative velocity range of approximately -10.5 to -17.5 m/s.

L_x (km)	t_e (days)	$c_{R3} - U$ (m/s)
6000	9.6	-10.4
6100	10.6	-10.7
6200	11.6	-11.1
6300	12.9	-11.4
6400	14.2	-11.8
6500	16.0	-12.1
6600	17.9	-12.5
6700	20.6	-12.9
6800	23.6	-13.2
6900	27.6	-13.6
7000	32.2	-14.0
7100	39.6	-14.3
7200	51.0	-14.7
7300	67.2	-15.1
7400	97.4	-15.5
7500	173	-15.8
7600	700	-16.2
7700	-	-16.6

North Pacific blocking which ~~is~~ 6000 to 7000 km according to Fig. 4.12.

Recomputed predictions for the full model with $L_y=120°$ and $U_T=8$ m/s showed an improvement in the growth rates as was seen with model 4. As given in Table 13, all waves in the 6000 to 7000 km range lie within the 10.5 to 17.5 m/s range for U and could conceivably undergo stationary amplification with e-folding times ranging from 10 days at the lower end to roughly one month at the upper extreme.

CHAPTER 5

SUMMARY AND CONCLUSIONS

In this investigation a linear two-level baroclinic model was formulated which incorporated a self-determining variable static stability. The attraction of this model was that the adiabatic-frictionless form of the equations contained certain invariant energy and vorticity properties which were desirable. Sensible heat exchange and frictional effects were then introduced in the equations as perturbation features within the steady-state current flow.

Harmonic solutions, independent of latitude or assigned a simple meridional wavelength variation, were assumed for the perturbation quantities. A cubic frequency equation was obtained and solved for varying conditions of current flow. Analysis of the resulting phase velocity response curves showed that:

(i) adiabatic-frictionless flow yielded a band of unstable waves with maximum instability at shorter wavelengths; such flow also exhibited a longwave cutoff, above which wave amplification was not possible.

(ii) sensible heat exchange reduced the instability of the unstable waveband at short and intermediate wavelengths while increasing the instability of longer waves.

(iii) friction diminished the instability of the perturbation field at all wavelengths except in two narrow regions found at the extremes of the unstable waveband.

(iv) simultaneous inclusion of friction and sensible heat exchange created the greatest reduction in the amount of instability available for short to medium length waves, but resulted in a longwave cutoff of longer proportions than that found with adiabatic-frictionless flow; coincident with this the propagation speeds of the longer unstable waves were significantly slower.

(v) the instability and wave speeds of the long waves increased as the meridional wavelength of the perturbations decreased.

The stability of the perturbation field was also subject to changes in the steady-state flow. Most notable were the effects of using larger vertical wind shear values and shifting the x-axis to higher latitudes both of which created increased instability in the waves. A reduction in the atmospheric mean stability produced more instability at shorter wavelengths, but had appreciably less effect at longer wavelengths.

An initial-value technique was employed to determine the wave amplitude and phase characteristics of the various perturbation quantities. Numerical solutions supported the findings of the stability analysis and indicated lesser wave amplification and slower wave speeds as wavelengths increased. It was also established that the thermal wave necessarily lags the stream function during unstable wave growth and that, conversely, the static stability leads the stream function wave. Maximum downward vertical velocity and the location of maximum surface heat exchange to the atmosphere were found between the ridge and the downstream trough position.

It had been suggested in a previous study by White and Clark (1975) that regional North Pacific blocking activity owed its existence to its marine environment and the presence of sensible heat flux. The present study investigated the space and time scales of the unstable baroclinic long waves which were predicted by the theory. Using representative mean winter values for the zonal wind and vertical wind shear, the numerical values indicated that stationary unstable wave amplification having similar characteristic growth rates and wavelengths as North Pacific blocking ridges was possible when sensible heating was present. Agreement between the numerical results and observed values was improved if:

(a) the vertical wind shear in the mid-troposphere was marginally above its long term mean value;

(b) the perturbation field was given a single

meridional wavelength of 120° of latitude.
In the absence of sensible heat exchange stationary wave growth was possible, but not realistic because of the extremely slow growth rates involved. Certainly such amplification would not occur on the same space or time scales as observed with blocking ridges.

The position of maximum heat exchange within the modelled atmosphere supported the spatial correlations between blocking and anomalous heat flux distributions over the North Pacific ocean found by White and Clark (1975). They found that anomalous surface sensible heating was negatively correlated with the position of a blocking ridge formation. The initial-value technique indicated that at a wavelength of 7000 km maximum perturbation heating in the surface layer of the atmosphere occurred some 50° upstream of the trough position during development, thereby putting maximum cooling just downstream of the ridge.

The concept of blocking ridge activity as a form of baroclinic instability would not seem unreasonable from the results which were found in this study. However, the theory presented can only cast inferences on the development of blocking formations. Linear perturbation theory can say very little of the ridge's ability for sustained existence without apparent further amplification. The model used in this study excluded a major mechanism for heating in the atmosphere – that of latent heat release. Further investigation is required to determine in what way this heat source would influence the numerical predictions. Orographic and land/sea constraints were also neglected in the modelling. Kikuchi (1971) found in his numerical studies that mountains and land-sea distribution played a major role in the longitudinal position of the blocking action, but were not necessary for the creation of blocking waveforms. In addition, his study indicated that numerically-simulated blocking ridges had a tendency for longer duration if terrain effects were included in the modelling. Additional theoretical approaches are required, however, to substantiate the role that orographic effects play in the scheme of blocking formations.

REFERENCES

Baur, E., 1974: Dispersion of tracers in the atmosphere and ocean: Survey and comparison of experimental data. *J. Geophys. Res.*, *79*, 789-795.

Berggren, R., E. Bolin and C.G. Rossby, 1949: An aerological study of zonal motion, its perturbations and breakdown. *Tellus*, *1*, 14-37.

Budyko, M.I., 1956: *The Heat Balance of the Earth's Surface* (Translation prepared by the Office of Technical Services, U.S. Dept. of Commerce: Teplovoi balans zemnoi poverkhnosti, Gidrometeorologischekoe izdatel stvo.) Leningrad, 256 pp.

Businger, J.A., 1973: Turbulent transfer in the atmospheric surface layer. *Workshop on Micrometeorolgy*. Publ. by the American Meteor. Soc., Boston, Ma., 67-98.

Charney, J.G., 1947: The dynamics of long waves in a baroclinic westerly current. *J. Meteor.*, *4*, 135-163.

——————, 1948: On the scale of atmospheric motions. *Geofys. Publikasjoner*, *17*, 17 pp.

——————, 1959: On the theory of the general circulation of the atmosphere. *The Atmosphere and the Sea in Motion*. The Rockefeller Institute Press, 178-193.

——————, and N.A. Phillips, 1953: Numerical integration of the quasigeostrophic equations for barotropic and simple baroclinic flows. *J. Meteor.* *10*, 71-99.

Clark, N.E., 1967: *Report on an Investigation of Large-scale Heat Transfer Processes and Fluctuations of Sea-surface Temperature in the North Pacific Ocean*. Ph.d. dissertation, M.I.T., 148 pp.

Cressman, G.P., 1960: Improved terrain effects in barotropic forecasts. *Mon. Wea. Rev.*, *88*, 327-342.

Crutcher, H.L., (ed.), 1959: *Upper Wind Statistics of the Northern Hemisphere*. Issued by the Chief of Naval Operations.

——————, 1961: *Meridional Cross-sections, Upper Winds Over the Northern Hemisphere*. Tech. Paper No. 41, National Weather Records Center, Asheville, N.C.

______________, and J.M. Merserve, 1970: Selected Level Heights, Temperatures and Dew Points for the Northern Hemisphere. NAVIAR Publ. 50-1C-52, Washington, D.C.

Deardorff, J.W., 1967: Empirical dependence of the eddy coefficient for heat upon stability above the lowest 50 m. J. of App. Met., 6, 631-643.

Derome, J. and A. Wiin-Neilson, 1971: The response of a mid-latitude model atmosphere to forcing by topography and stationary heat sources. Mon. Wea. Rev., 99, 564-576.

Döös, B.R., 1962: The influence of exchange of sensible heat with the earth's surface on the planetary flow. Tellus, 14, 133-147.

Egger, J., 1976: The Linear response of a hemispheric two-level primative equation model to forcing by topography. Mon. Wea. Rev. 104, 351-364.

Gates, W.L., 1961: The stability properties and energy transformations of the two-layer model of variable static stability. Tellus, 13, 460-471.

___________, 1975: The January global climate simulated by a two-level general circulation model: A comparison with observation. J. Atmos. Sci., 32, 449-477.

Hage, K.D., 1964: Particle Fallout and Dispersion Below 30 km in the Atmosphere. Rep. SC-DC-64-1463, National Tech. Inform. Service, Springfield, Va.

Haltiner, G.J., 1967: The effects of sensible heat exchange on the dynamics of baroclinic waves. Tellus, 19, 183-198.

______________, 1971: Numerical Weather Predication. John Wiley and Sons, Inc., New York, 317 pp.

______________, and D.E. Calverly, 1965: The effect of friction on the growth and structure of baroclinic waves. Quart. J. Roy. Meteor. Soc., 91, 209-214.

______________, and F.L. Martin, 1957: Dynamical and Physical Meteorolcgy. McGraw-Hill Book Co., New York, 470 pp.

Holopainen, E.O., 1961: On the effect of frictiom on baroclinic waves. Tellus, 3, 363-367.

Kikuchi, Y., 1969: Numerical simulation of the blocking process. *J. Meteor. Soc. Japan*, *47*, 29-45.

__________, 1971: Influence of mountains and land-sea distributions on blocking action. *J. Meteor. Soc. Japan (special issue)*, *49*, 564-572.

Kraus, E. and R. Morrison, 1966: Local interaction between the sea and the air at monthly and annual time scales. *Quart. J. Roy. Meteor. Soc.*, *92*, 114-127.

Lorentz, E.N., 1960: Energy and numerical weather prediction. *Tellus*, *12*, 364-373.

Lumley, J.L. and H.A. Panofsky, 1964: *The Structure of Atmospheric Turbulence*. John Wiley and Sons, Inc., New York. 239 pp.

Namias, J., 1950: The index cycle and its role in the general circulation. *J. Meteor.*, *7*, 130-139.

__________, 1959: Recent seasonal interactions between North Pacific Ocean waters and the overlying atmospheric circulation. *J. Geophys. Res.*, *64*, 631-645.

Phillips, N.A., 1956: The general circulation of the atmosphere: A numerical experiment. *Quart. J. Roy. Meteor. Soc.*, *82*, 123-164.

Rex, D.F., 1950a: Blocking action in the middle troposphere and its effect upon regional climate: I. An aerological study of blocking action. *Tellus*, *2*, 196-211.

__________, 1950b: Blocking action in the middle troposphere and its effect upon regional climate: II. The climatology of blocking action. *Tellus*, *2*, 295-301.

__________, 1951: The effect of Atlantic blocking action upon European climate. *Tellus*, *3*, 100-112.

Rossby, C.G., 1950: On the dynamics of certain types of blocking waves. *J. Chinese Geophys. Soc.*, *2*, 1-13.

White, W.B. and N.E. Clark, 1975: On the development of blocking ridge activity over the Central North Pacific. *J. Atmos. Sci.*, *32*, 489-502.

Yeh, T., 1949: On energy dispersion in the atmosphere. *J. Meteor.*, *6*, 1-16.